Beta-complex versus Alpha-complex: Similarities and Dissimilarities

Donguk Kim, Mokwon Lee, Youngsong Cho, and Deok-Soo Kim

Abstract—The beta-complex is a construct derived from the Voronoi diagram of spherical balls of arbitrary radii and has proven a powerful capability for proximity reasoning among spherical balls in three-dimensional space. Important applications related to molecular shapes in structural/computational molecular biology have been correctly, efficiently, and conveniently solved in the unified framework of the beta-complex and the Voronoi diagram. The beta-complex is a generalization of the ordinary alpha-complex. However, there are similarities and dissimilarities between the two complexes and it is necessary to correctly understand these similarities and dissimilarities to choose the right complex to solve application problems at hand. This paper presents the similarities and dissimilarities between these constructs and illustrates the consequence of the dissimilarity in application problems from both theoretical and practical points of view using examples of atomic arrangements.

Index Terms—Voronoi diagram of spheres, additively-weighted Voronoi diagram, power diagram, quasi-triangulation, alpha-complex, beta-complex, proximity

1 Introduction

Particles are everywhere in the universe. Many problems in science and engineering are frequently related to particles, particularly to their proximity. Interpolating a surface through a point cloud is an immediate example [1], [2], [3], [4]. Emerging application areas include structual/computational molecular biology and material science where the three-dimensional arrangement of spherical atoms, hereafter referred to as a molecule, with arbitrary radii is fundamental. It is well-known that molecular function is determined by molecular structure and molecular shape is one of the most critical factors of molecular structure. While there have long been mathematical and computational efforts to understand and characterize molecular shape, most studies have used rather ad hoc approaches such as Monte Carlo simulation or space enumeration using grid points. Only recently have researchers attempted to use computational geometry constructs with theoretical foundations [5], [6], [7], [8], [9], [10], [11].

As far as we know, the ordinary Voronoi diagram of points where the points were atom centers was first used for molecules by Bernal and Finney to analyze the packing characteristics of amorphous atomic arrangements in 1967 [12] and then by Richards to define the boundary surface of molecule, now called the Connolly surface, in 1974 [13], [14]. The ordinary Voronoi diagram may indeed be good enough for problems that can be sufficiently modelled by a set of monosized spherical atoms, and it is still popular for solving such types of molecular structure problems. However, if a problem requires to incorporate the size difference among atoms in more detail, a more advanced computational structure beyond this type of Voronoi diagram is necessary.

In this regard, Gellatly and Finney, in 1982, employed the radical plane as the bisector between two atoms after experiencing a "vertex error" caused by a mismatch among arbitrarily translated Voronoi bisectors (i.e., Voronoi edges in $\mathbb{R}^2$ and Voronoi faces in $\mathbb{R}^3$) of the ordinary Voronoi diagram for points [15]. The power diagram, formalized by Aurenhammer in 1987 [16] and also called the Laguerre diagram, is the formalization of using radical planes as the bisectors between nearby atoms. However, Goede et al. reported, in 1997, that the power diagram is not sufficient for certain molecular problems such as the computation of atomic volume distribution in molecules and suggested the need for a Voronoi diagram of polysized atoms, also called the additively weighted Voronoi diagram [17], [18]. Will, in 1999, indeed used the Voronoi cells in the Voronoi diagram of atoms to compute the distribution of the volume of atomic occupation in proteins [19]. In 2000, Kim et al. reported an algorithm for computing the Voronoi diagram of circles with arbitrary radii in the plane [20], [21], [22] and, in 2016, Lee et al. reported a robust incremental algorithm for the circle Voronoi diagram [23]. In 2004, Kim et al. reported its three dimensional counterpart, the algorithms for the Voronoi diagram of atoms: the edge-tracing algorithm [24], [25] and the region-expansion algorithm [26] both stored the topology in

- *D. Kim is with the Department of Industrial and Management Engineering, Gangneung-Wonju National University, Wonju 26403, South Korea. E-mail: donguk@gwnu.ac.kr.*
- *M. Lee and D.-S. Kim are with the School of Mechanical Engineering, HYU-HPSTAR-CIS High Pressure Research Center, Hanyang University, Seoul 04763, South Korea. E-mail: mwlee.vdrc@gmail.com, dskim@hanyang.ac.kr.*
- *Y. Cho is with the Voronoi Diagram Research Center, HYU-HPSTAR-CIS High Pressure Research Center, Hanyang University, Seoul 04763, South Korea. E-mail: yscho.vdrc@gmail.com.*

Manuscript received 4 Dec. 2017; revised 7 Sept. 2018; accepted 15 Sept. 2018. Date of publication 18 Oct. 2018; date of current version 4 Mar. 2020. (Corresponding author: Deok-Soo Kim.) Recommended for acceptance by L. Liu. Digital Object Identifier no. 10.1109/TVCG.2018.2873633

a radial-edge data structure [27]. They have shown that the Voronoi diagram can be used for solving various molecular biology problems such as the Connolly surface [28], interaction interface [29], etc. [30], [31].

On the other hand, efforts to devise more convenient and efficient computational constructs derived from the Voronoi diagram have also been made. In 1983, the concept of the alpha-shape in a plane was proposed as a generalization of the convex hull of a point set by Edelsbrunner et al. [32], and Edelsbrunner and Mücke [33], in 1994, extended the two-dimensional alpha-shape to the three-dimensional one and reported an algorithm based on the Delaunay triangulation, i.e., the dual of the ordinary Voronoi diagram. In an effort to account for the size differences among atoms, Edelsbrunner also reported the weighted alpha-shape using the regular triangulation, the dual of the power diagram [34]. The weighted alpha-shapes have been used in many protein related problems. Winter et al. reported a review paper discussing (weighted) alpha-shape as well as beta-shape and applications to various protein related problems [35]. Gameiro et al. proposed a method to measure the softness of a protein by persistence diagrams which is extracted from the weighted alpha-complexes [36]. Recognizing that the generalization of the alpha-shape concept through the Voronoi diagram of atoms could be useful for solving various shape-related problems in molecular biology, Kim et al. devised the concept of the beta-shape where "beta" implies "β lending" using a rolling ball of radius β [37]. Based on the quasi-triangulation, which is the dual structure of the Voronoi diagram of atoms, they developed the beta-complex theory and showed that many molecular structure problems could be efficiently solved within the unified framework of the beta-complex [38].

In visualization and computer graphics community, many studies on molecular structures have been reported to visualize and define molecular structures. Visualization methods for molecular surfaces from molecular dynamics simulations are reported in [39], [40]. Grottel et al. reported a framework called MegaMol for visualizing large scale molecular system including large molecular surfaces [41]. Lindow et al. proposed a new type of molecular surface called ligand excluded surface which is defined by a few geometric configurations of a ligand [42]. Detecting voids and tunnels in molecules is known to be important to study molecular behavior. Lindow et al. reported an extraction and visualization method of molecular tunnels, which is based on the Voronoi diagram of atoms [11]. Kim et al. also reported a method to recognize molecular voids and tunnels using the Voronoi diagram of atoms and its derived construct beta-complex [43], [44]. Their method also computes geometric properties such as volume and surface area of voids and tunnels accurately and efficiently. Fig. 1 shows such an example of detected tunnel of a protein by Kim et al.'s method. Byska et al. developed AnimoAminoMiner which visualize tunnel properties of a protein over time in molecular dynamics simulation [45].

Being a generalization of the ordinary alpha-complex, the beta-complex has both similarities and dissimilarities with the weighted alpha-complex. For users to choose an appropriate one for solving their problems at hand, it is necessary to correctly understand these similarities and dissimilarities.

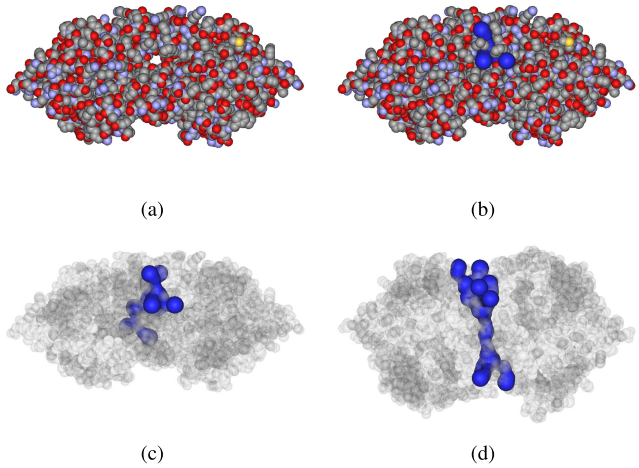

Fig. 1. A recognized tunnel of a protein (PDB code: 1jd0) using the beta-complex. The tunnel (blue) allows a spherical probe of radius 1.4Å to freely move through the protein (A movie file showing the 3D views of this example is presented as a supplemental material, which can be found on the Computer Society Digital Library at http://doi.ieeecomputersociety.org/10.1109/TVCG.2018.2873633/): (a) Notice the direct (white) hole through the protein modeled by 4,699 spherical atoms, (b) the protein with the recognized tunnel (blue), (c) the tunnel with the partially transparent atoms, and (d) another view of 90-degree rotation around the horizontal axe.

Through contacts with users of our software library, we learned that there were misunderstandings that caused difficulties for researchers to make a right choice. For this reason, we report this paper to point out the differences as clearly as possible. Voronoi Diagram Research Center (VDRC, http://voronoi.hanyang.ac.kr) freely provides application programs, such as BetaVoid [44], BetaMol [46] and BetaConcept [47], for molecular applications based on the Voronoi diagram, the quasi-triangulation, and the beta-complex.

In this paper, an "atom" denotes a spherical ball with a center and a radius. We prefer the "Voronoi diagram of atoms" to the "additively weighted Voronoi diagram" because it is more intuitive for researchers in application areas, particularly in molecular biology and material science. We denote "(weighted) alpha-complex" to be both ordinary alpha-complex and weighted alpha-complex. Voronoi diagrams and triangulations are sometimes referred to as primary structures and dual structures, respectively.

This paper is organized as follows: Section 2 presents the basics of the Voronoi diagrams of the different types and their corresponding dual structures. Section 3 presents the basics of three main structures: the ordinary alpha-complex, the weighted alpha-complex, and the beta-complex. Section 4 compares the different distance functions used for the beta-complex and the (weighted) alpha-complex and their influence on the topological structures. Section 5 summarizes the similarities and dissimilarities between the beta-complex and the (weighted) alpha-complex. Section 6 compares the beta-shape and the (weighted) alpha-shape. Section 7 presents the consequence of the dissimilarities between the beta-complex and the weighted alpha-complex from the view point of application problems. Then, the paper concludes.

2 Primal and Dual Structures

Let $P = \{p_1, p_2, \ldots, p_n\}$ be a set of point sites in $\mathbb{R}^d$. The *Voronoi cell* of p_i is defined as $\mathrm{VC}(p_i) = \{x \in \mathbb{R}^d \mid d(x, p_i) \leq$

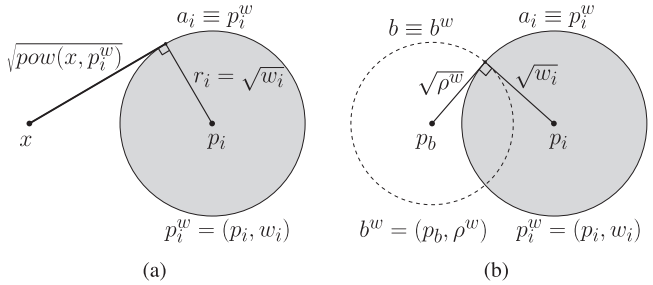

Fig. 2. Relationship between a weighted point and an atom: (a) the power distance from a point x to a weighted point $p_i^w = (p_i, w_i)$, and (b) the two weighted point $b^w = (p_b, \rho^w)$ and p_i^w are orthogonal.

$d(x, p_j),\ i \neq j\}$ where $d(x, p)$ is the Euclidean distance between two points x, $p \in \mathbb{R}^d$. The *Voronoi diagram* of P is defined as $\mathrm{VD}(P) = \{\mathrm{VC}(p_1), \mathrm{VC}(p_2), \ldots, \mathrm{VC}(p_n)\}$ where the connectivity among the vertices, edges, faces, and cells of the Voronoi diagram in $\mathbb{R}^3$ is appropriately represented [48], [49]. Efficient and robust codes for computing $\mathrm{VD}(P)$ in $\mathbb{R}^2$ and $\mathbb{R}^3$ are available [50], [51], [52]. The dual of $\mathrm{VD}(P)$ is the Delaunay triangulation $\mathrm{DT}(P)$ and the transformation between $\mathrm{VD}(P)$ and $\mathrm{DT}(P)$ takes linear time in the number of simplexes. $\mathrm{DT}(P)$ is a simplicial complex. The number of vertices, edges, faces, and tetrahedral cells in $\mathrm{DT}(P)$ is bounded by $\mathrm{O}(n^2)$ in $\mathbb{R}^3$ [33].

Suppose that $p_i \in P$ is now assigned a weight $w_i \geq 0$. Let $P^w = \{p_1^w, p_2^w, \ldots, p_n^w\}$ where $p_i^w = (p_i, w_i)$. Let $\mathrm{PC}(p_i^w) = \{x \in \mathbb{R}^d \mid pow(x, p_i^w) \leq pow(x, p_j^w),\ i \neq j\}$ be the power cell of p_i^w where $pow(x, p_i^w) = d(x, p_i)^2 - w_i$ is the power distance from x to p_i^w. $\mathrm{PD}(P^w) = \{\mathrm{PC}(p_1^w), \mathrm{PC}(p_2^w), \ldots, \mathrm{PC}(p_n^w)\}$ is called the *power diagram* where the connectivity among the vertices, edges, faces, and cells in $\mathbb{R}^3$ are appropriately represented [16]. The power distance $pow(x, p_i^w)$ from a point x to a weighted point p_i^w has the following geometric interpretation: $p_i^w = (p_i, w_i)$ corresponds to a spherical atom $a_i = (p_i, r_i)$ with the center p_i and the radius $r_i = \sqrt{w_i}$. See Fig. 2a. Then, $pow(x, p_i^w)$ is the square of the tangential distance from x to a_i. The power bisector between p_i^w and p_j^w is a set of points $\{x \in \mathbb{R}^d \mid pow(x, p_i^w) = pow(x, p_j^w)\}$, and it forms a plane. Hence, every power cell is bounded by planar facets. The power bisector passes through $\partial a_i \cap \partial a_j$ if $a_i \cap a_j \neq \emptyset$ where ∂a_i denotes the boundary of a_i, and therefore it translates toward the smaller weighted point from the perpendicular bisector of p_i and p_j. Hence, the power diagram reflects atom size difference from the power distance sense, although no accuracy in Euclidean distance sense. A power cell $\mathrm{PC}(p_i^w)$ may not contain p_i. This problem occurs frequently to cause computational trouble in biomolecules around hydrogen [17]. The dual of a power diagram PD is called a regular triangulation RT and is a simplicial complex [53]. The transformation between PD and RT takes linear time with respect to the number of simplexes [48]. The number of vertices, edges, faces, and tetrahedral cells in RT are bounded by $\mathrm{O}(n^2)$ in $\mathbb{R}^3$ [49], [54].

The Voronoi diagram of atoms is defined as follows. Let $A = \{a_1, a_2, \ldots, a_n\}$ be a set of atoms where $a_i = (p_i, r_i)$ is a sphere with the center p_i and radius r_i. We assume that an atom is not fully contained by another. Let $\mathrm{VC}(a_i)$ denote the Voronoi cell of a_i defined as $\mathrm{VC}(a_i) = \{x \in \mathbb{R}^d \mid d(x, p_i) - r_i \leq d(x, p_j) - r_j,\ i \neq j\}$. Then, the Voronoi diagram of atoms A is defined as $\mathrm{VD}(A) = \{\mathrm{VC}(a_1), \mathrm{VC}(a_2), \ldots, \mathrm{VC}(a_n)\}$ where the connectivity among the topological entities are appropriately represented by an efficient data structure like a radial-edge data structure. Since the initial concept and following studies of the Voronoi diagram of atoms [16], [19], [55], [56], [57], its robust and efficient computation has long been a challenge. Kim et al. reported two algorithms with $O(n^3)$ time complexity in the worst-case: the edge-tracing algorithm [24], [25] and the region-expansion algorithm [26]. They have shown that this Voronoi diagram is powerful for solving various geometry-related problems in molecular biology [29], [30], [44], [58], [59], [60], [61]. While this Voronoi diagram has been discussed since mid-eighties, its dual was never discussed until Kim et al. [62] proposed the quasi-triangulation QT in 2006. QT is not necessarily a simplicial complex. It is a quasi-*triangulation* because most simplexes locally satisfy the simplicial complex condition and is a *quasi*-triangulation because there may be some, mostly very few, simplexes which violate the simplicial complex condition and their influences are mostly local. The condition that causes the violation is called an *anomaly* and has been well-studied [63]. For the details, see [62], [64].

3 Beta-complexes and (Weighted) Alpha-complexes

3.1 Ordinary Alpha-complexes

The following paragraph, quoted from [33], explains alpha-shapes very intuitively yet clearly for a point set P and a nonnegative real number α: "Think of $\mathbb{R}^3$ filled with Styrofoam and the points of P made of more solid material, such as rock. Now imagine a spherical eraser with radius α. It is omnipresent in the sense that it carves out Styrofoam at all positions where it does not enclose any of the sprinkled rocks, that is, points of P. The resulting object will be called the *alpha-hull*. To make things more feasible we straighten the surface of the object by substituting straight edges for the circular ones and triangles for the spherical caps. The obtained object is the alpha-shape of P." If $\alpha = \infty$, the alpha-shape is identical to the convex hull of P. If $\alpha = 0$, the alpha-shape is reduced to the point set P itself. An alpha-shape may contain triangular faces and edges and may be non-manifold due to possible handles, interior voids, and dangling edges (The weighted alpha-shape and the beta-shape also have this property). The boundary of an alpha-shape is a simplicial complex because it is a subset of the Delaunay triangulation DT. This type of alpha-shape for a point set P is called an ordinary alpha-shape. The subset of the DT contained within an ordinary alpha-shape, including the simplexes on its boundary, is the *ordinary alpha-complex*, which is also a simplicial complex.

The formal definition of ordinary alpha-complex is given in [33] and we rewrite as the following.

Definition 1 (Ordinary alpha-complex). *Let $T \subset P$ be the set of points constituting a simplex $\sigma_T \in \mathrm{DT}$, and let ρ_T be the radius of the smallest sphere b_T touching all the points in T. Then,* the ordinary alpha-complex of P with a parameter α *is defined as a subcomplex of* DT *that contains $\sigma_T \in \mathrm{DT}$ if (1) $\rho_T < \alpha$ and b_T is empty, or (2) σ_T is a face of another simplex in the alpha-complex.*

The algorithm for alpha-complexes is based on a set of simple rules about the conditions for each simplex σ in DT [33]. The rule determines whether $\sigma \in \mathrm{DT}$ will be a member of the resulting alpha-complex for a given parameter α by checking its state among four possibilities: exterior, singular, regular, or interior. A simplex σ is exterior if it does not belong to the corresponding alpha-complex; σ is singular if it belongs to the boundary of the alpha-shape but it does not bound the interior of the alpha-shape; σ is regular if it belongs to the boundary of the interior of the alpha-shape; σ is interior if it belongs to the interior of the alpha-shape. For the details, see [33].

3.2 Weighted Alpha-complexes

The weighted alpha-complex is an effort to incorporate atom size into an ordinary alpha-complex. Each point $p_i \in P$ is assigned a weight w_i. Then, the weighted alpha-complex is extracted from the regular triangulation RT of P^w [34]. The edges and faces of RT, which are *determined* to be larger than a spherical eraser, are removed from the regular triangulation. Then, what is left is the weighted alpha-complex and the space occupied by the weighted alpha-complex defines the weighted alpha-shape. Both the weighted alpha-complexes and the boundary of the weighted alpha-shapes are also simplicial complexes. Weighted alpha-shapes are non-manifold in general.

The formal definition is given in [34], and we rewrite as the following by changing some symbols for notational consistency.

Definition 2 (Weighted alpha-complex). *Let $T \subset P^w$ be the set of weighted points constituting a simplex $\sigma_T \in \mathrm{RT}$. Let $b_T^w = (p_b, \rho_T^w)$ be the weighted point with the minimum weight ρ_T^w that is orthogonal to all $p^w \in T$. Let b_T^w be orthogonal to $p^w = (p, w)$ if $d(p, p_b)^2 - \rho_T^w - w = 0$. Fig. 2b shows such an orthogonal case between two weighted points. The weighted point b_T^w is called conflict-free if $d(p, p_b)^2 - \rho_T^w - w < 0$ for all weighted point $p^w \in P^w - T$. Then,* the weighted alpha-complex of a parameter α^w *is defined as a subcomplex of* RT *that contains $\sigma_T \in \mathrm{RT}$ if (1) $\rho_T^w < \alpha^w$ and b_T^w is conflict-free, or (2) σ_T is a face of another simplex in the weighted alpha-complex.*

The rules for extracting ordinary alpha-complexes applies to weighted alpha-complexes.

The power diagram is based on the power distance, and the weighted alpha-complex is extracted from the power diagram. Hence, the weighted alpha-complex takes the size variations among the spherical atoms into account in the power distance sense. The power diagram and the weighted alpha-complex can correctly provide with the information on the intersections among atoms, and the weighted alpha-complex is used to compute the volume and the surface area of an atomic complex [65]. However, when two atoms do not intersect, the weighted alpha-complex cannot properly convey the Euclidean distance between the two atoms.

3.3 Beta-complexes

To correctly account for the atom size difference of molecules in the Euclidean distance, the concept of the *beta-complex* was proposed initially in 2006 [37]. Think of $\mathbb{R}^3$ filled with styrofoam and some spherical rocks of arbitrary radii are scattered within. Carving out the styrofoam with an omnipresent spherical eraser of radius β will result in a blended geometric object called the *beta-hull*. Since the eraser is omnipresent, there can be interior voids and tunnels as well. The Connolly surface in biology is indeed equivalent to the beta-hull of a molecule [66], [67]. The spherical eraser is called a *beta-probe*. Suppose that we have a beta-hull of an atom set A. We straighten the surface of the beta-hull by substituting straight edges for circular ones and triangles for spherical caps where the vertices are the centers of the atoms contributing to the boundary of the beta-hull. The straightened object bounded by the planar facets is the *beta-shape* corresponding to the beta-probe. The subset of the quasi-triangulation QT of A contained within and on the boundary of the beta-shape is the *beta-complex*. A beta-complex is extracted from QT by removing the edges and faces determined to be larger than a probe. The extraction of beta-complexes from a QT is simply done by watching parsing tables given in [38]. The beta-complex is not necessarily a simplicial complex but the beta-shape boundary is a simplicial complex.

The formal definition of beta-complex is given in [38], and we rewrite as the following.

Definition 3 (Beta-complex). *Given a set A of atoms in $\mathbb{R}^3$, let $T \subset A$ be the set of atoms constituting a simplex $\sigma_T \in \mathrm{QT}$. Let b_T be the smallest empty sphere simultaneously tangent to each atom in T with the same orientation as σ_T, and let ρ_T be the radius of b_T. Then,* the beta-complex of a parameter β *is defined as the simplex set $\{\sigma_T, \sigma_{T'} \mid T' \subset T, 1 \leq |T| \leq 4,$ for all possible $T \subset A$ where $\rho_T \leq \beta\}$.*

Fig. 3 shows a set of eight two-dimensional atoms and two instances of the beta-complex for two different probe radii β's in the plane. Fig. 3a shows the beta-hull for a probe of radius $\beta_1 > 0$. Fig. 3b shows the quasi-triangulation of the atom set: All the vertices, edges, and triangular faces (which are blank for visualization convenience) belong to the member of the quasi-triangulation. Figs. 3c and 3d show the beta-complex and beta-shape corresponding to β_1, respectively. Note that the smallest atom a_3 corresponds to a non-manifold vertex in the beta-shape because a dangling edge is connected to the vertex. Figs. 3e and 3f show the beta-complex and beta-shape, respectively, for a probe of radius $\beta_2 < \beta_1$ where the blank triangle does not belong to a member of both beta-complex and beta-shape. New non-manifold vertices and dangling edges are created in the beta-shape for β_2. Note that both beta-complexes, and thus both beta-shapes as well, are computed from the unique Voronoi diagram. The eight atoms are as follows: $a_1 = (x_1, y_1, r_1) = (132, 304, 52)$, $a_2 = (180, 140, 40)$, $a_3 = (228, 216, 16)$, $a_4 = (236, 320, 38)$, $a_5 = (296, 232, 31)$, $a_6 = (308, 312, 59)$, $a_7 = (344, 252, 33)$, and $a_8 = (416, 180, 44)$. This atom set is also used for other illustrations later on.

The beta-complex is very powerful for molecular structure problems due to the following dual properties. *Accurate proximity*: The beta-complex has correct proximity information among all the atoms both within and on the boundary of molecule where the boundary is defined by a probe. *Concise abstraction*: The beta-complex maintains the proximity information among the nearest neighbors of each atom in the topology among simplexes. The beta-shape is used for the efficient computation of the Connolly surface [58], the

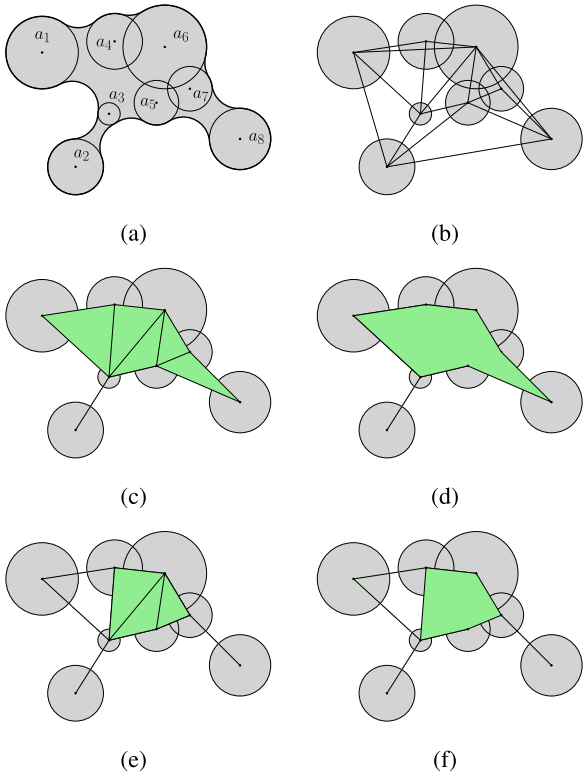

Fig. 3. Relationship among the beta-hull, beta-complex, beta-shape, and quasi-triangulation: (a) the beta-hull for β_1, (b) the quasi-triangulation (all blank triangles belong to the member), (c) the beta-complex for β_1, (d) the beta-shape for β_1, (e) the beta-complex for $\beta_2 < \beta_1$ (the blank triangle does not belong to the member), and (f) the beta-shape for β_2.

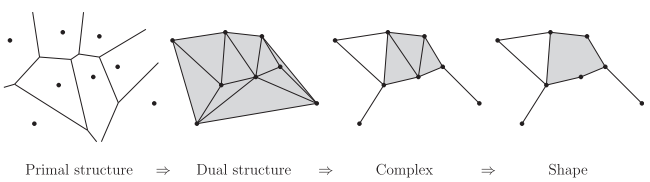

Fig. 4. The transformation from the primal structure of a point set to the dual structure to the complex and to the shape in $\mathbb{R}^2$. The shaded and blank triangles are of significance and will be later explained.

recognition of pockets [68], the recognition of molecular voids and tunnels [69], etc; the beta-complex is used for molecular mass properties such as the volume and boundary area [70].

3.4 Voronoi Diagrams, Triangulations, Complexes, and Shapes

The primal structures (i.e., Voronoi diagrams) transform to the dual structures (i.e., triangulations). Complexes are extracted from the dual structures, and the boundaries of (the space taken by) the complexes define the shapes. Fig. 4 shows this process for the case of a point set in a plane.

Fig. 5 summarizes the transformation in Fig. 4 for each complex structure: Computation of the Voronoi diagram, transformation to its triangulation, and extraction of the complex and shape. We emphasize that the fidelity of each complex to the Euclidean distance increases from the ordinary alpha-complex to the weighted alpha-complex and to the beta-complex. This is obvious because, for a given set of atoms with arbitrary radii, the Euclidean fidelity increases

Voronoi diagram of atoms	⇒	Quasi-triangulation	⇒	Beta-complex	Euclidean fidelity increases
Power diagram	⇒	Regular triangulation	⇒	Weighted alpha-complex	
Ordinary Voronoi diagram	⇒	Delaunay triangulation	⇒	Ordinary alpha-complex	

Fig. 5. The transformations for the (weighted) alpha-complexes and the beta-complex. The euclidean fidelity increases from the ordinary alpha-complex to the weighted alpha-complex and to the beta-complex.

from the ordinary Voronoi diagram to the power diagram and to the Voronoi diagram of atoms.

The time complexities for computing the three types of Voronoi diagrams are all $O(n^3)$ in the worst case, where n is the number of input generators in $\mathbb{R}^3$. As the combinatorial complexities of all three types of Voronoi diagrams are $O(n^2)$ in $\mathbb{R}^3$ [16], [48], [49], there can be $O(n^2)$ vertices, edges, and faces in the Voronoi diagram in $\mathbb{R}^3$. However, our experiments show that the computation time of the Voronoi diagrams for most molecular structures from the protein data bank (PDB) is strongly linear in the number of atoms. The worst case scenario usually does not occur for biomolecules because atoms are constrained to be connected due to the chemical bonds and are clustered around each other due to the van der Waals force, electrostatic force, hydrogen bonding, etc. The actual computation time requirement is in the order of the ordinary Voronoi diagram of points, the power diagram, and the Voronoi diagram of atoms. For all three structures, the dual transformation takes $O(m)$ time in the worst case, where m is the number of simplexes in the dual structure and $m = O(n)$ in most applications we encountered. It is noteworthy that the dual transformation consists of only symbolic operations and thus is very fast. Fig. 6a shows the computation time of QT for 100 protein data in PDB. Each green diamond in the graph denotes computation time to apply the dual transformation in addition to the time to compute the Voronoi diagram of atoms. The graph shows linear time behavior and approximately 1,600 atoms are processed in a second to obtain QT on an ordinary desktop computer. The extraction of a complex takes $O(\log m)$ time for simple queries if the complex is binary-searched from a sorted list. A discussion of more general queries is presented in [71].

As the size of biomolecules such as proteins is usually big, i.e., tens of thousand or hundreds of thousand, the computation speed of 1,600 atoms/sec for constructing QT may not be sufficiently fast for practical applications. Hence, we have developed an approach to preprocess to construct the Voronoi diagram structure of molecules and store the dual structure in a database, called QTDB, to upload to solve applications. The file format is called a quasi-triangulation file format (QTF) which stores the topology information of QT [72]. Once a QTF file is available in QTDB, it can be quickly uploaded (and can be transformed to the corresponding Voronoi diagram in the linear time about the number of simplexes, if necessary). The red rectangles in each Fig. 6a and 6b represent the loading time of the QTs of the 100 protein structures from QTDB: We compare it with the computation time of RT and DT as shown in Fig. 6b. RT and DT were computed using CGAL [51] of version 4.0.2 in our experiment. Fig. 6b shows that the loading time of QT from QTDB is comparable to the construction of RT. Hence, we propose to preprocess each PDB file to generate a QTF file and store in QTDB to solve application problems using

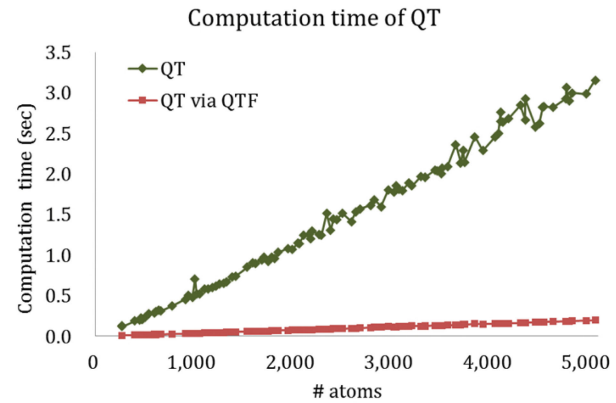

(a)

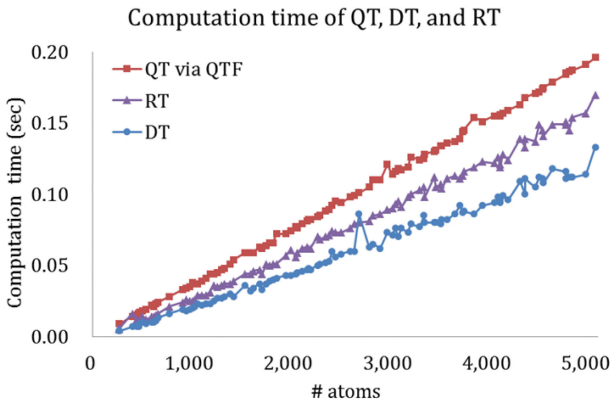

(b)

Fig. 6. Computation time for QT, DT, and RT in $\mathbb{R}^3$ of 100 protein data in PDB. QT is computed by the Voronoi diagram of atoms using edge-tracing algorithm. DT and RT are computed by CGAL [51] (version 4.0.2). QT via QTF is obtained by loading QTF file from QTDB. This experiment was done by a PC of Intel Core 2 Duo 3.0 GHz CPU and 2 GB RAM. (a) Computation time of QT: QT from scratch and QT by loading QTF file. (b) Computation time of QT via QTF, RT, and DT.

QT. Details on QTF is presented in [72]. We estimate that the RT construction algorithm processes approximately 30,000 atoms per second. As the edge-tracing algorithm of the Voronoi diagram can process approximately 1,600 atoms per second, the construction of RT is roughly 19 times faster than that of QT.

4 Differences Due to Different Distance Functions

We now compare the influence of the difference between the Euclidean distance and the power distance on the proximity among atoms. Fig. 7 shows the cases where an edge is created between two particles in the ordinary alpha-complex (Figs. 7a and 7b) and the beta-complex (Figs. 7c and 7d). Fig. 7a shows that an edge is created between the two points p_1 and p_2 when the alpha-probe (shown by the dashed circle) is sufficiently large so that it can *touch* the two points simultaneously. Fig. 7b is an alternative interpretation of this case that the two circles enlarged by the radius α and centered at the two points *intersect* each other. Figs. 7c and 7d shows a corresponding situation for the beta-complex. Let $a_i' = (p_i, r_i + \beta)$ be the enlarged atom from $a_i = (p_i, r_i)$. In

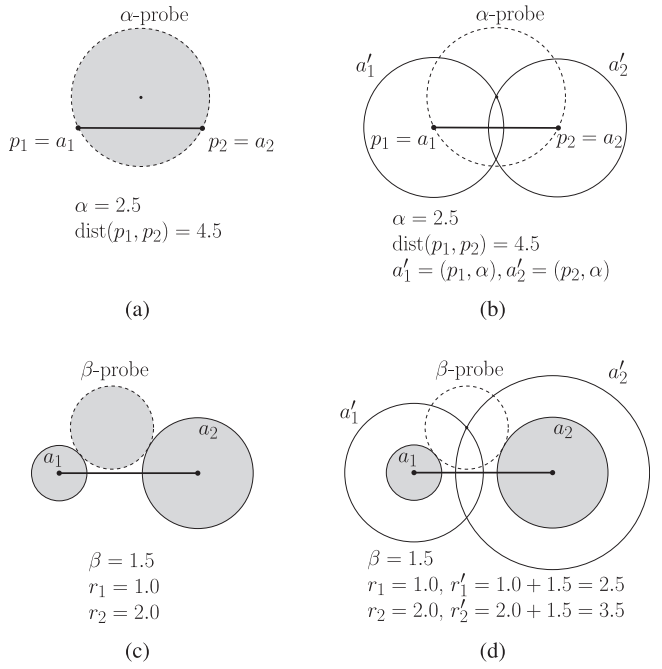

Fig. 7. The conditions when the edges of an ordinary alpha-complex and a beta-complex are created. (a) An edge created with respect to the alpha-probe, (b) an edge created with respect to enlarged disks, (c) an edge created with respect to a beta-probe, and (d) an edge created with respect to enlarged disks.

Fig. 7c, an edge is created between the centers of two atoms a_1 and a_2 because the beta-probe simultaneously touches the two atoms, and in Fig. 7d, the two circles a_1' and a_2' enlarged by the beta-probe radius β intersect each other. Therefore, the creation of an edge simplex in both the ordinary alpha-complex and beta-complex is intuitive.

While the parameters α and β are the *radii* of the alpha- and beta-probes for the ordinary alpha-complex and beta-complex, respectively, the parameter α^w of the weighted alpha-complex used in [34] is the *weight* of the probe. Then, $\sqrt{\alpha^w}$ corresponds to the radius of the spherical probe in the weighted alpha-complex. This is similar to the fact that the weighted point $p_i^w = (p_i, w_i)$ in the power diagram is interpreted as a spherical atom whose radius is $\sqrt{w_i}$ as shown in Fig. 2. Therefore, the interpretation of α^w of the weighted alpha-complex in relation to a probe radius is different from that of the parameter α of an ordinary alpha-complex. Hereafter, we will use α as the unified parameter to denote the probe radius of both the ordinary and weighted alpha-complexes for notational consistency and convenience. If distinction is required, we use α_{ord} and α_{wei} as parameters of ordinary alpha-complexes and weighted alpha-complexes, respectively, i.e., $\alpha_{\mathrm{wei}} = \sqrt{\alpha^w}$. This interpretation shall be clear in the context.

While the creation of an edge is intuitive in the beta-complex as shown in Figs. 7c and 7d, it is not so in the weighted alpha-complex. In the weighted alpha-complex, an edge is created if the alpha-probe of radius α can intersect two atoms at a right angle simultaneously [34]. This condition can be detected by checking if the two enlarged atoms, whose radii $\tilde{r}_i$ are given as

$$\tilde{r}_i = \sqrt{r_i^2 + \alpha^2}, \tag{1}$$

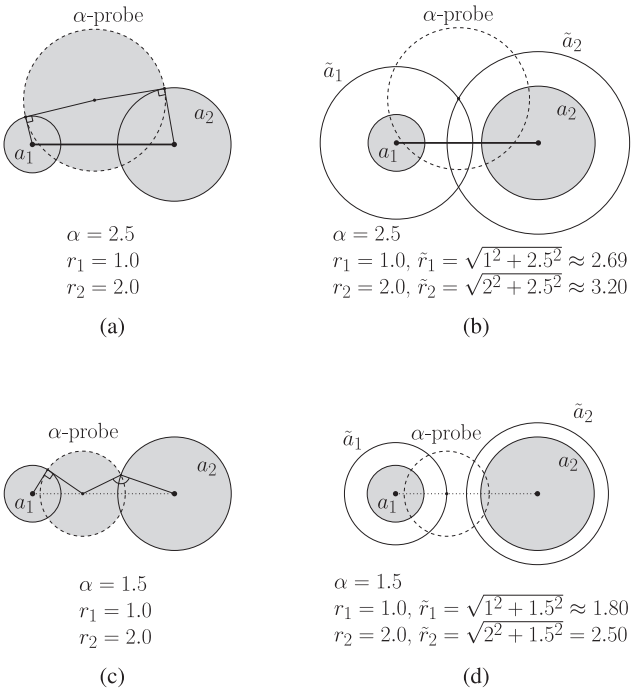

Fig. 8. The interpretation of the α-value in the weighted alpha-complex: α is the radius of the alpha-probe, and $r_i = \sqrt{w_i}$ and $\tilde{r}_i = \sqrt{r_i^2 + \alpha^2}$, $i = 1, 2$. The alpha-probe intersects a_1 and a_2 simultaneously at the right angle iff the boundaries of $\tilde{a}_1$ and $\tilde{a}_2$ intersect. The intersection points become the centers of the alpha-probe.

TABLE 1
Summary of the Parameter and Enlarged Atom's Radius for Each Complex Structure

Complex	Parameter (probe radius)	Radius of enlarged atom
Beta-complex	β	$r'_i = r_i + \beta$
Weighted alpha-complex	$\alpha_{\text{wei}} (= \sqrt{\alpha^w})$	$\tilde{r}_i = \sqrt{r_i^2 + \alpha_{\text{wei}}^2}$
Ordinary alpha-complex	α_{ord}	$r'_i = r_i + \alpha_{\text{ord}}$

The subscripts "wei" and "ord" of parameter α's are omitted if its meaning is clear.

$i = 1$ and 2, intersect or not. Fig. 8a shows an example of an alpha-probe and two atoms in the weighted alpha-complex in $\mathbb{R}^2$. Note that the alpha-probe intersects both atoms at a right angle, and therefore an edge simplex is defined between the centers of the two atoms. Let $\tilde{a}_i = (p_i, \tilde{r}_i)$ be the enlarged atom from a_i where $\tilde{r}_i$ is given by Eq. (1). Then, $\tilde{a}_1$ and $\tilde{a}_2$ intersect each other and thus an edge is created in the weighted alpha-complex. In this case, the alpha-probe intersecting both atoms at a right angle is centered at one of the two intersections between $\partial\tilde{a}_1$ and $\partial\tilde{a}_2$, as shown in Fig. 8b. Figs. 8c and 8d shows a case that an edge is not defined between the two atoms. Note that the α-probe cannot be located so that it intersects the boundaries of *both* atoms at a right angle even if it can simultaneously intersect both atoms. Be aware that $\tilde{a}$'s are atoms enlarged by different amounts, whereas a''s are those enlarged by a constant amount as shown in Fig. 10b. The parameters and the enlarged radius for each complex structure are summarized in Table 1.

It is obvious that the radius $\tilde{r}$ of each enlarged atom increases monotonically as α increases. For a fixed α, however, the amount of radius difference decreases as r increases, which means that the parameter α has less influence on larger atoms.

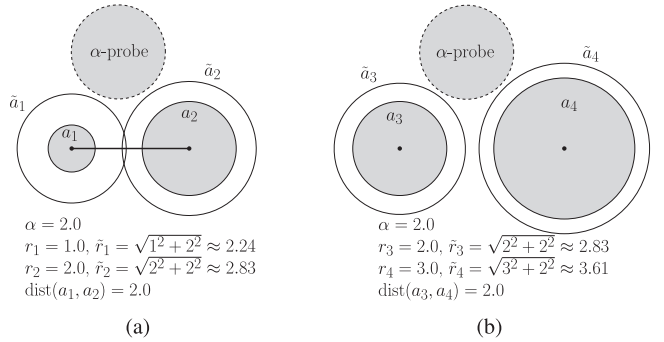

Fig. 9. Same-sized bottlenecks between atoms and a same α-value leading to different consequences in the weighted α-complex. (a) An edge is created between the centers of a_1 and a_2, and (b) no edge is created between a_3 and a_4.

Lemma 1. *Let $\delta_i = \tilde{r}_i - r_i$ be a radius increment when $\alpha > 0$ is fixed. Then, $\delta_i > \delta_j$ iff $r_i < r_j$.*

Proof. Let $\delta(r, \alpha) = \sqrt{r^2 + \alpha^2} - r$. Then,

$$\frac{d}{dr}\delta(r, \alpha) = \frac{r - \sqrt{r^2 + \alpha^2}}{\sqrt{r^2 + \alpha^2}}, \tag{2}$$

is always negative if $\alpha > 0$. Therefore, $\delta(r, \alpha)$ decreases as r increases. □

Therefore, given an α-value in the weighted alpha-complex, the smaller the atom radius r is, the larger the radius increment δ is in the enlarged atom. Fig. 8b clearly verifies Lemma 1: $r_1 < r_2$ and therefore $\delta_1 > \delta_2$. Also we know that radius increment $\delta(r, \alpha)$ is non-linear with respect to r and/or α from Eq. (2).

Fig. 9 shows two atomic arrangements: the atoms in Fig. 9a are smaller than those in Fig. 9b. Let $\text{dist}(a_i, a_j)$ be the Euclidean minimum distance between the two atoms a_i and a_j. In both figures, $\text{dist}(a_1, a_2) = \text{dist}(a_3, a_4) = 2.0$ and both alpha-probe radii are kept identically as 2.0. In this configuration, $\tilde{a}_1$ and $\tilde{a}_2$ intersect each other but $\tilde{a}_3$ and $\tilde{a}_4$ do not. Therefore, an edge is created between a_1 and a_2. However, no edge is created between a_3 and a_4 even if the minimum distances are same. In this sense, the weighted alpha-complex may not be very intuitive for applications where a bottleneck distance plays an important role. See Section 7 for the consequence of this property in applications. Therefore, this observation leads to the following lemma that easily generalizes to higher dimensions.

Lemma 2. *Consider a set $A = \{a_1, a_2\}$ in the plane, and an alpha-probe is given with $\alpha \geq \text{dist}(a_1, a_2)/2$. An edge between a_1 and a_2 of the weighted alpha-complex may not be defined, whereas the edge is always defined in the beta-complex of $\beta = \alpha$.*

We observe the geometric implication of α in the weighted alpha-complex in relation to the beta-complex. Both Figs. 10a and 10b have an identical set of two atoms, $A = \{a_1, a_2\}$, and they correspond to the weighted alpha-complex and the beta-complex, respectively. In Fig. 10, both the probe radii are identical, i.e., $\alpha = \beta = 1.5$. From the figure, we know that the influence of α is much less than β

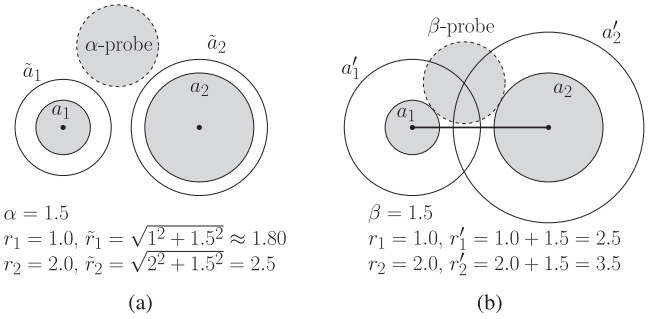

Fig. 10. For the same α and β values, α-value has less influence than β-value: (a) no edge is defined in the weighted alpha-complex because $\tilde{a}_1$ and $\tilde{a}_2$ has no intersection, and (b) an edge is defined between a_1 and a_2 in the beta-complex.

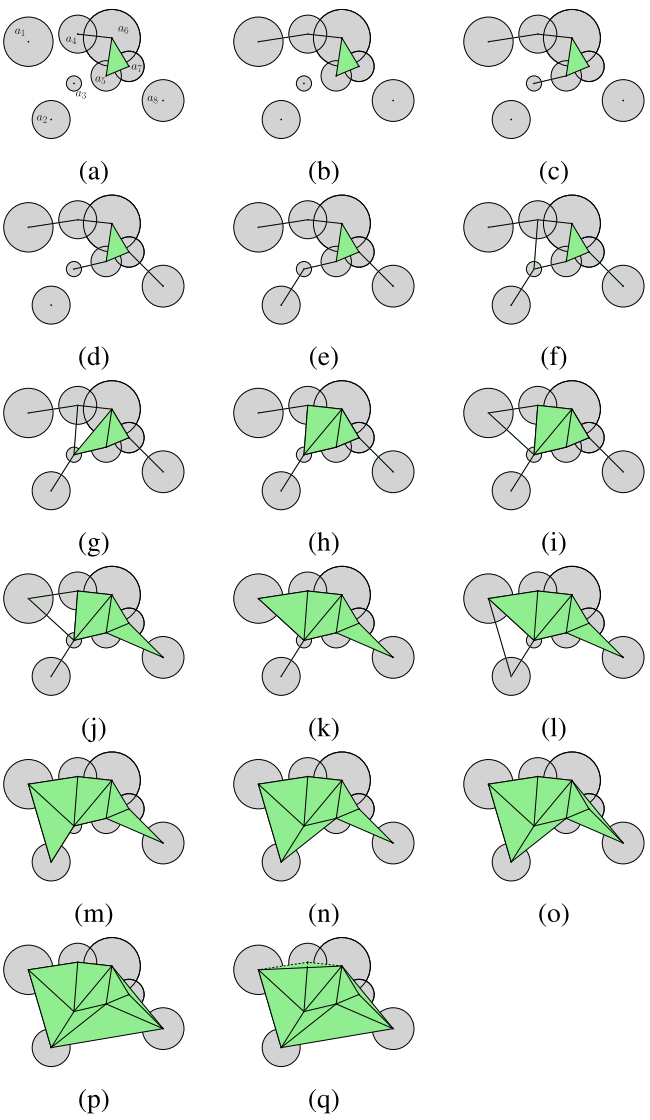

Fig. 11. The evolution of beta-complexes of the atom set A as the probe radius β increases from 0 to ∞. The set A is identical to the one used in Fig. 3.

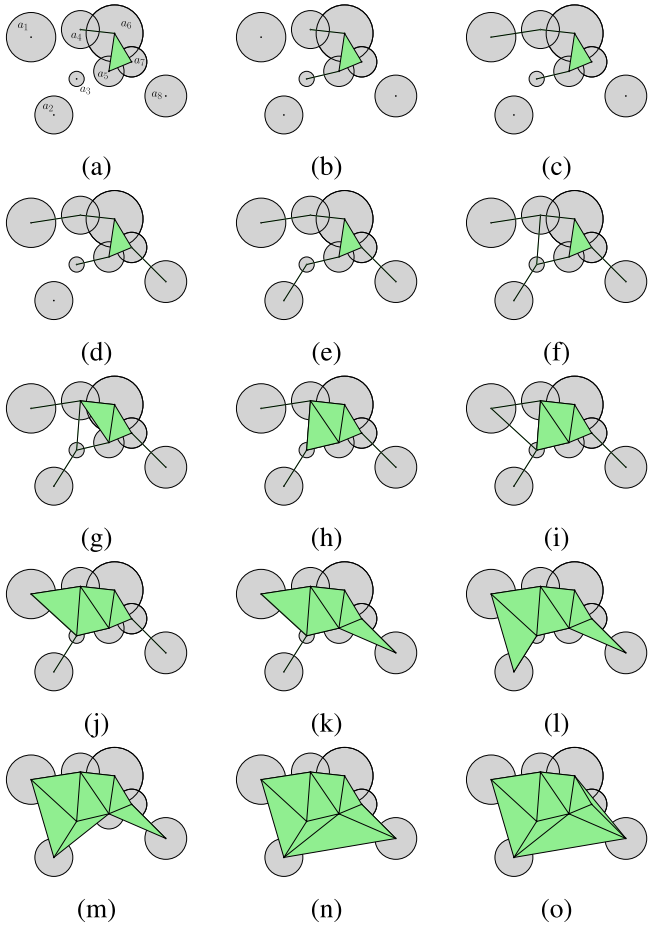

Fig. 12. The evolution of the weighted alpha-complexes as the probe radius α increases from 0 to ∞. The set A is identical to the one used in Fig. 3.

even if $\alpha = \beta$. In Fig. 10a, the two enlarged atoms $\tilde{a}_1$ and $\tilde{a}_2$ do not intersect, and therefore the alpha-probe cannot intersect both atoms at a right angle. On the other hand, the beta-probe in Fig. 10b touches both atoms simultaneously and the enlarged atoms a'_1 and a'_2 intersect each other. Therefore, for the given probe of radius 1.5, an edge is created in the beta-complex, whereas no edge is created in the weighted alpha-complex. The beta-complex is obviously more intuitive.

It is informative to observe the evolution of the beta-complex and the weighted alpha-complex for an identical set of atoms as the parameters β and α increase from 0 to ∞, respectively. Figs. 11 and 12 show such evolutions of the beta-complex and the weighted alpha-complex, respectively. Each figure enumerates all possible complexes as the parameter increases continuously. This atom set is identical to the one used in Fig. 3.

When a beta-complex is defined by a probe of radius $\beta = 0$, it is called a *zero beta-complex*. Similarly, the beta-shape of $\beta = 0$ is called a *zero beta-shape*. Similar convention applies to (weighted) alpha-complexes and (weighted) alpha-shapes. Fig. 11a shows the zero beta-complex: There is a triangle because three atoms a_5, a_6, and a_7 have a common intersection; there is a dangling edge because the corresponding two atoms a_4 and a_6 intersect each other; each of the other four isolated atoms a_1, a_2, a_3, and a_8 maps to a disconnected vertex. Fig. 11b introduces a new edge between a_1 and a_4 because $\mathrm{dist}(a_1, a_4)$ is the smallest among all the possible pairs of the non-intersecting atoms. A similar procedure sequentially produces Fig. 11c through 11f by adding one edge at a time as the beta-probe continues to grow. Fig. 11g has a new triangle $\triangle p_3 p_5 p_6$ because the correspondingly enlarged atoms a'_3, a'_5, and a'_6 have a common intersection. Continuing this procedure, the beta-complex evolves

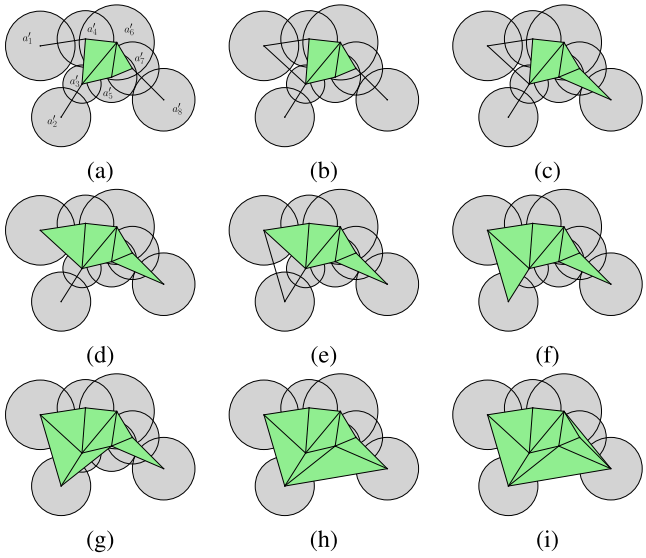

Fig. 13. The evolution of the weighted alpha-complexes for the enlarged atoms A' as the probe radius α increases from 0 to ∞. The radius of each atom in A' is increased by 28 from the radius of each corresponding atom in A where A is the one used in Fig. 3.

by adding one new simplex, either an edge or a triangle, at a time as the beta-probe grows. Note that the last triangle added in Fig. 11q has two dotted edges. Each dotted edge is shared by two triangles and is interior topologically, but it is on the boundary geometrically.

Fig. 12a shows the zero weighted alpha-complex ($\alpha = 0$). Note that this weighted alpha-complex is identical to the zero beta-complex in Fig. 11a. This is because both complexes convey the same information of the intersection among the atoms. Immediately after this initial complex, the next weighted alpha-complex in Fig. 12b becomes different from the beta-complex in Fig. 11b. Observe that the new edge in Fig. 12b is added between a_3 and a_5. This is because the sizes of the atoms a_1 and a_4 are larger than those of a_3 and a_5, and thus the enlargement of a_1 and a_4 is much smaller than that of a_3 and a_5. Fig. 12c through 12f are identical to those of Fig. 11c through 11f, respectively. Then, the weighted alpha-complex in Fig. 12g is different from the beta-complex in Fig. 11g in the way a new triangle is defined. Thus, this difference inherits to the succeeding weighted alpha-complexes to the last one. Note that the last triangle added in Fig. 12o is different from that in Fig. 11q and it does not have any dotted edge.

Fig. 13 shows the evolution of the weighted alpha-complex for the enlarged atom set A'. The radius of each atom $a'_i \in A'$ is increased by 28 from the radius of $a_i \in A$, $i = 1, 2, \ldots, 8$. This figure presents an interesting issue. Surprisingly, every weighted alpha-complex in Fig. 13 does not have an identical counterpart in Fig. 12. Instead, the weighted alpha-complexes from Fig. 13a through 13g are identical to the beta-complexes of Fig. 11h through 11n. In Figs. 13h and 11o, the newly added triangles are different. The complexes in both Figs. 13i and 11p are identical: This is the last step in the evolution of the weighted alpha-complex of A' but there is one more step for the beta-complex.

Fig. 14 shows the dual structures used in the previous three examples. Figs. 14a and 14b shows the quasi-triangulation and the regular triangulation of the same atom set A

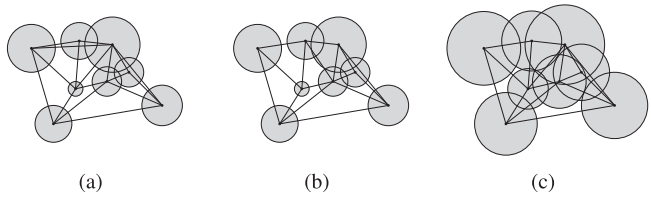

Fig. 14. Dual structures. (a) The quasi-triangulation of A, (b) the regular triangulation of A, and (c) the regular triangulation of A'.

from which the weighted alpha-complexes and the beta-complexes are extracted, respectively. Fig. 14c shows the regular triangulation of the enlarged atom set A' from which the weighted alpha-complexes in Fig. 13 are extracted. Note that the three triangulations are all different. These dual structures are entirely realized in all complexes where the probe size approaches infinity.

5 Beta-complexes versus (Weighted) Alpha-complexes

In this section, we compare properties of the beta-complexes and the (weighted) alpha-complexes. Let A be a set of atoms and P be the set of the atom centers in A.

5.1 Equal Radii of Atoms

If the radii of atoms in A are identical, both the beta-complex and the (weighted) alpha-complex have strong similarities.

Lemma 3. *Suppose that the radii of all the atoms in A are reduced to zero. Both the beta-complex and the weighted alpha-complex of A are identical to the ordinary alpha-complex of P if $\alpha = \beta$.*

Proof. When all the atoms in A have zero radius, both the quasi-triangulation and the regular triangulation reduce to the Delaunay triangulation DT(P). Hence, the simplexes constituting the beta-complex as well as the weighted alpha-complex are extracted from the same dual structure DT(P). In addition, both the beta-probe and alpha-probe have the same radius $\alpha = \beta$; and the intersection criteria are also identical since all the given atoms are points. Therefore, the resulting three complex structures are identical. □

In this paper, the identity of two structures means that both they have identical sets of vertices and the topologies among the vertices, edges, and cells are also identical. In other words, the sets of the vertices, edges, faces, and cells are all identical.

Lemma 4. *Suppose that the radii of all the atoms in A are identically r. Then, the beta-complex of A is identical to the ordinary alpha-complex of P if $\alpha = \beta + r$.*

Proof. Because all the atom radii in A are identically r, QT (A) and DT(P) are identical. It is obvious that the minimum tangent sphere of the atoms defining each simplex in the dual structure has a smaller radius by r than that of the atom centers. Hence the same simplex set is extracted from the dual structure if $\alpha = \beta + r$. □

A stronger equivalence condition follows.

Lemma 5. *Suppose that the radii of all the atoms in A are identically r. Then, the beta-complex of A is identical to the weighted*

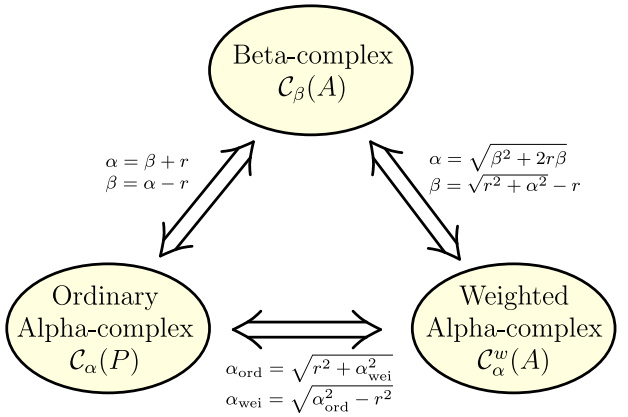

Fig. 15. (Equal radii) The transformation among the beta-complex, the alpha-complex, and the weighted alpha-complex when all the atoms have the same radii r. "A $\Leftrightarrow$ B" means that A becomes identical to B when the proper one of the conditions on the shoulder is satisfied, and vice versa.

alpha-complex of A with parameter $\alpha = \sqrt{\beta^2 + 2r\beta}$, and the weighted alpha-complex of A is identical to the beta-complex of A with parameter $\beta = \sqrt{r^2 + \alpha^2} - r$.

Proof. Because all the atom radii are r, QT(A) and RT(A) are identical to DT(P). For each simplex of the triangulation, each atom touches the beta-probe when $d = r + \beta$ where d is the distance between the atom center and the beta-probe. Similarly, each atom and the alpha-probe are orthogonal when $d^2 = r^2 + \alpha^2$. From the above equations, we obtain $(r + \beta)^2 = r^2 + \alpha^2$. Then, we get $\alpha = \sqrt{\beta^2 + 2r\beta}$ and $\beta = \sqrt{r^2 + \alpha^2} - r$. □

Lemma 6. *Suppose that the radii of all the atoms in A are identically r. Then, the ordinary alpha-complex of P with the parameter α_{ord} is identical to the weighted alpha-complex of A with the parameter α_{wei} if $\alpha_{\text{ord}} = \sqrt{\alpha^2_{\text{wei}} + r^2}$.*

Proof. By Lemma 5, the weighted alpha-complex is identical to the beta-complex if $\beta + r = \sqrt{\alpha^2_{\text{wei}} + r^2}$. In addition, by Lemma 4, the beta-complex is identical to the ordinary alpha-complex if $\alpha_{\text{ord}} = \beta + r$ holds. Hence, the ordinary alpha-complex is identical to the weighted alpha-complex if $\alpha_{\text{ord}} = \sqrt{\alpha^2_{\text{wei}} + r^2}$. □

Summary. Given that the radii of all the atoms in A are identically r with the set P of their centers, the beta-complex of A reduces to the ordinary alpha-complex of P if $\alpha_{\text{ord}} = \beta + r$, the beta-complex reduces to the weighted alpha-complex if $\alpha_{\text{wei}} = \sqrt{\beta^2 + 2r\beta}$, and the weighted alpha-complex reduces to the ordinary alpha-complex if $\alpha_{\text{ord}} = \sqrt{\alpha^2_{\text{wei}} + r^2}$. Fig. 15 shows this observation.

5.2 Unequal Radii of Atoms

When the atoms have arbitrary radii, the beta-complex and the weighted alpha-complex of an atom set A may differ from each other even if the parameters α and β are identical. This is because their dual structures, i.e., the quasi-triangulation and the regular triangulation for the same set A, are not identical, as illustrated in Fig. 14.

Lemma 7. *Let $A' = \{a'_1, a'_2, \ldots, a'_n\}$ be the set of atoms where $a'_i = (p_i, r_i + \beta)$. The regular triangulations of A and A' are not necessarily identical, whereas the quasi-triangulations of A and A' are identical.*

Proof. Suppose that there are two atoms $a_1 = (p_1, r_1)$ and $a_2 = (p_2, r_2)$, and there are two enlarged atoms $a'_1 = (p_1, r_1 + \beta)$ and $a'_2 = (p_2, r_2 + \beta)$. Let $\text{diff}_{\text{Euc}}(a_1, a_2)$ be the difference between the Euclidean distances to the atoms a_1 and a_2 from an arbitrary point p. Then, $\text{diff}_{\text{Euc}}(a_1, a_2) = \{d(p, p_1) - r_1\} - \{d(p, p_2) - r_2\}$, and $\text{diff}_{\text{Euc}}(a'_1, a'_2) = \{d(p, p_1) - (r_1 + \beta)\} - \{d(p, p_2) - (r_2 + \beta)\}$. Due to $\text{diff}_{\text{Euc}}(a_1, a_2) = \text{diff}_{\text{Euc}}(a'_1, a'_2)$, we know that the value β does not affect the distance difference from an arbitrary point to the atoms, and therefore VD(A) and VD(A') become identical as well as the corresponding quasi-triangulations. Similarly, let $\text{diff}_{\text{pow}}(a_1, a_2) = pow(p, a_1) - pow(p, a_2)$ be the difference between the power distances to the atoms a_1 and a_2 from an arbitrary point p. Then, $\text{diff}_{\text{pow}}(a_1, a_2) = \{d(p, p_1)^2 - r_1^2\} - \{d(p, p_2)^2 - r_2^2\}$ and $\text{diff}_{\text{pow}}(a'_1, a'_2) = \{d(p, p_1)^2 - (r_1 + \beta)^2\} - \{d(p, p_2)^2 - (r_2 + \beta)^2\}$. From the equation $\text{diff}_{\text{pow}}(a_1, a_2) - \text{diff}_{\text{pow}}(a'_1, a'_2) = 2\beta(r_1 - r_2) \neq 0$, we know that the radius increment β influences the difference in distance, and therefore PD(A) and PD(A') are different for $\beta \neq 0$. Therefore, the corresponding regular triangulations may not be identical. □

Figs. 14b and 14c show an example of Lemma 7.

Lemma 8. *Let $A' = \{a'_1, a'_2, \ldots, a'_n\}$ be the set of atoms where $a'_i = (p_i, r_i + \beta)$. Then, the beta-complex of A with parameter β is not necessarily identical to the zero weighted alpha-complex of A'.*

Proof. The beta-complex may not be a simplicial complex, whereas the zero weighted alpha-complex of A' is always a simplicial complex. □

The following lemma states the uniqueness property of complexes.

Lemma 9. *Given a set A of atoms with arbitrary radii, some beta-complex may not have an identical weighted alpha-complex, and some weighted alpha-complexes may not have an identical beta-complex.*

From Figs. 11 and 12, we see that only five beta-complexes in Figs. 11a, 11c, 11d, 11e, and 11f are identical to the weighted alpha-complexes in Figs. 12a, 12c, 12d, 12e, and 12f, respectively. Each of the other twelve beta-complexes and ten weighted alpha-complexes is unique and does not have an identical counterpart.

Lemma 10. *The zero beta-complex of A is not necessarily identical to the zero weighted alpha-complex of A.*

Proof. The zero beta-complex may not be a simplicial complex, whereas the zero weighted alpha-complex of A' is always a simplicial complex. □

6 Beta-shapes versus (Weighted) Alpha-shapes

Since shape structure is defined from the corresponding complex structure, all the identity conditions among complex structures, i.e., Lemmas 3 through 6, also hold among the shape structures. We will omit such lemmas for the

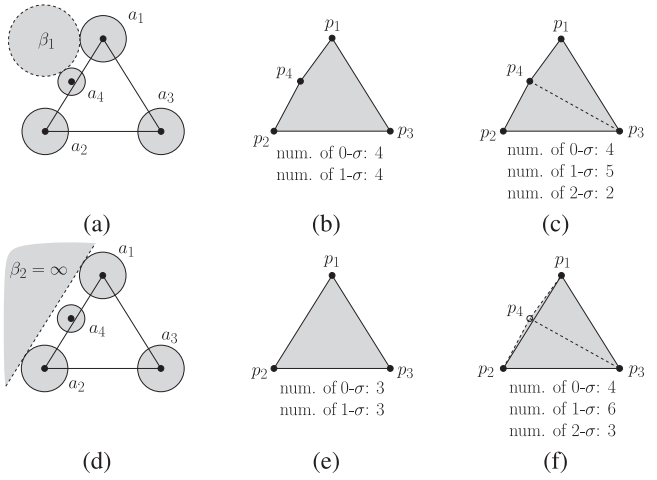

Fig. 16. Beta-shapes and beta-complexes for four atoms in the plane. (a) An atom set, (b) and (c): (a)'s beta-shape and beta-complex corresponding to β_1, respectively; (d) the identical atom set as before, (e) and (f): (d)'s beta-shape and beta-complex for $\beta_2 = \infty$, respectively.

shape structures in this section. Summarizing similarity among complex structures, all the identity conditions hold only when the atoms have identical radii, but such conditions do not hold when atoms have arbitrary radii among complex structures. However, identity conditions exist between the beta-shape and the weighted alpha-shape even if atoms have arbitrary radii.

Fig. 16 shows beta-shapes and beta-complexes for two beta-values where $0 < \beta_1 < \beta_2 = \infty$ for given atom set $A = \{a_1, a_2, a_3, a_4\}$. In this figure, p_4, the center of a_4, is located outside the triangle $\triangle p_1 p_2 p_3$. The dashed lines in the beta-complexes in Figs. 16c and 16f denote the interior-state edges, and the hollow circle denotes the interior-state vertex. Note that the interior-state edges and vertices are *topologically* interior, and thus they are shared by other simplexes and do not exposed topologically to the exterior. As illustrated in Fig. 16f, some interior-state edges and vertices are located outside the corresponding beta-shape. Such a case occurs only in quasi-triangulations (thus in the beta-complexes) but not in Delaunay or regular triangulations (thus in the (weighted) alpha-complexes). However, the boundary of a beta-shape consists of only singular and regular simplexes and thus they always form a simplicial complex.

Lemma 11. *The boundary of a beta-shape is a simplicial complex.*

Because the beta-shape boundary forms a simplicial complex, we can use this property for efficient solution for the problems in close relation to the molecular boundary such as the Connolly surface construction, van der Waals surface (area) calculation, offset surface (area) computation, and so on.

The following equivalence relationship holds regardless whether atoms have identical radii or not.

Lemma 12. *The zero beta-shape of A and the zero weighted alpha-shape of A are identical.*

Proof. When $\beta = 0$, the beta-shape boundary defines the intersections among the boundary of the atoms in model A. Similarly, when $\alpha = 0$, the boundary of the weighted alpha-shape defines the same intersection information of the same model. Therefore, the beta-shape and the weighted alpha-shape are identical when $\alpha = \beta = 0$ because A has a unique boundary. □

Lemma 12 in fact states that both the beta-shape and the weighted alpha-shape convey identical information regarding the intersections among the atoms exposed to the outside. This is due to the fact that both the Voronoi diagram and the power diagram provide an identically correct information of the intersections among atoms.

From Figs. 11 and 12, we see that each of the beta-shapes in Figs. 11b, 11g, 11l, 11o, and 11q has no identical weighted alpha-shape counterpart in Fig. 12, and each of the weighted alpha-shapes in Figs. 12b, 12g, 12j, and 12n has no identical beta-shape counterpart in Fig. 11. In other words, some beta-shapes and some weighted alpha-shapes are unique in their respective structures. Hence, the following lemma holds.

Lemma 13. *Given a set A of atoms with arbitrary radii, some beta-shape of A may not have an identical weighted alpha-shape of A, and some weighted alpha-shape of A may not have an identical beta-shape of A.*

However, for each beta-shape, there exists an identical weighted alpha-shape instance for a set of enlarged atoms by an appropriate amount, say δ. As the beta-shape has the offset-invariant property which facilitates a powerful capability for applications, it is useful to find the value of δ. The following lemma is from [37].

Lemma 14. *Let A be a set of atoms with arbitrary radii. Let $A' = \{a'_1, a'_2, \ldots, a'_n\}$ be the set of atoms where $a'_i = (p_i, r_i + \beta)$. Then, the beta-shape of A with the parameter β is identical to the zero weighted alpha-shape of A'. Let $\tilde{A} = \{\tilde{a}_1, \tilde{a}_2, \ldots, \tilde{a}_n\}$ be the set of atoms where $\tilde{a}_i = (p_i, \sqrt{r_i^2 + \alpha^2})$. Then, the weighted alpha-shape of A with the parameter α is identical to the zero beta-shape of $\tilde{A}$.*

Let $\mathscr{S}_\alpha$ be the ordinary alpha-shape of a point set P. Let $\mathscr{S}^w_\alpha$ and $\mathscr{S}_\beta$ be the weighted alpha-shape and the beta-shape of an atom set A, respectively.

Lemma 15. *Let A be a set of atoms with arbitrary radii. Then, $\mathscr{S}_\beta$ of A for an arbitrary value of $\beta \geq 0$ is computed from the unique quasi-triangulation of A, whereas the equivalent $\mathscr{S}^w_\alpha$ can be computed by the regular triangulation which needs to be re-computed for the enlarged atoms A' by the amount β.*

Hence, in the weighted alpha-shape, the regular triangulation needs to be computed again whenever a new value of β is given. On the other hand, the beta-shape can be immediately computed from the unique quasi-triangulation whatever value of β is. The computational advantage of the beta-shape approach is significant particularly when multiple beta-shapes of A should be used for large molecules.

Fig. 17 summarizes the equality relationships between the beta-shape and the weighted alpha-shape from Lemmas 12 and 14. From the figure, we know that the beta-shape of A with a probe radius β can also be obtained by the weighted alpha-shape approach by computing zero weighted alpha-shape of an enlarged atom set A' by the amount of β. This implies that if a program which is equipped with only the weighted alpha-shape but a user needs to solve problems based on the beta-shape for a particular β, the equivalence relationship in Fig. 17a can be used, but in the cost of

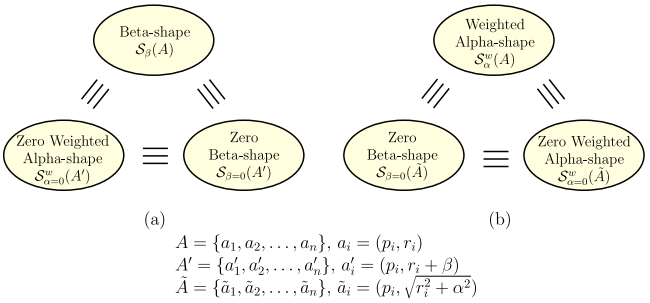

Fig. 17. Equality conditions among the beta-shapes and weighted alpha-shapes. (a) The equivalence condition between the beta-shape and the others, and (b) the equivalence condition between the weighted alpha-shape and the others.

re-computing the regular triangulation for A'. On the other hand, suppose that a user is allowed to use a program with the beta-shape capability only but needs to have a capability of the weighted alpha-shape for a particular α. Then, the equivalence relationship in Fig. 17b can be used, but in the cost of re-computing the quasi-triangulation for $\tilde{A}$. Therefore, the decision to choose which structure to use depends on the frequency of the use of each structure for solving application problems. As far as we have experienced and we have heard from researchers in various disciplines in science and engineering, most problems, if not all, are based on the Euclidean distance.

7 Consequences of the Dissimilarities in Applications

Weighted alpha-complexes are more powerful than beta-complexes for some problems. First, the weighted alpha-complex requires less computation than the beta-complex does. In our experiment, constructing the dual structure RT is approximately 19 times faster than QT whereas the extractions of the complex structures from RT and QT are similar once the RT and QT are available. Second, the weighted alpha-complex is a simplicial complex. Due to this property, the weighted alpha-complex as well as RT can be stored in a concise data structure without any special treatment handling exceptional cases. In addition, this property helps to make algorithms using weighted alpha-complexes simpler and researchers can use already proven properties about simplicial complexes in their application problems. Third, the weighted alpha-complex and RT are much easier to implement because their primal structure, i.e., power diagram, consists of linear geometric elements such as line segments and planes. In fact, power diagrams and RT are already available in several well-known programming libraries like CGAL in public.

However, dissimilarities between beta-complexes and weighted alpha-complexes have important consequences. Important applications arise in atomic arrangements which can be easily solved by the beta-complex but with weighted alpha-complexes, either i) they cannot be solved efficiently or ii) they cannot be solved correctly by the weighted alpha-complex. In this section, we show a few examples for readers better understanding of the dissimilarities.

7.1 Consequences on the Efficiency to a Solution

Given a molecule A consisting of atoms with arbitrary radii, the locus of the center of a spherical probe of a fixed radius that touches A from outside is called the offset surface. Computing the offset surface is one of the classic problems in geometric modeling community.

Problem 1 (Offset Problem). *Given a set A of atoms with arbitrary radii, compute the offset surface of A by the offset amount δ.*

Since the offset surface is the boundary of the union of the enlarged atoms from A by δ, this problem can be easily and efficiently solved by the beta-complex as follows. Given the quasi-triangulation of A, we extract the beta-shape of $\beta = \delta$ which has necessary and sufficient information to compute the correct offset boundary. Efficient computation of the volume and surface area for a molecule and its offsets using the beta-complex was reported [70].

The situation, however, is quite different for the weighted alpha-complex. The power diagram knows only the intersections among atoms but does not know about the Euclidean proximity among non-intersecting atoms. Because the weighted alpha-shape inherits this property, any problem requiring the Euclidean proximity among non-intersecting atoms has to be transformed into an intersection problem among appropriately enlarged atoms. Hence, to compute offset surface by weighted alpha-complex, it is necessary to produce an enlarged molecule A' that consists of the atoms enlarged by δ. Then, the power diagram of A' is computed and transformed to the regular triangulation $\mathrm{RT}(A')$ from which the zero weighted alpha-shape is extracted. This can also be explained by Lemma 14 in that the beta-shape of A with the parameter $\beta = \delta$ is identical to the zero weighted alpha-shape of A'.

Now, suppose that we want to compute another offset boundary of A by $\delta' \neq \delta$. In the beta-complex approach, we can use the same quasi-triangulation again to compute the beta-shape of $\beta = \delta'$ by Lemma 15. In the weighted alpha-complex approach, however, it is not possible to reuse $\mathrm{RT}(A')$, but repeating the previous procedure once more with δ' is inevitable. Hence, it is necessary to make another enlarged model A'' by δ', to compute $\mathrm{PD}(A'')$, to transform to $\mathrm{RT}(A'')$, and then to extract the zero weighted alpha-shape of A''.

A graphical example is shown in Fig. 18. Fig. 18a shows a two-dimensional molecule consisting of six atoms, its Voronoi diagram, and two correct offset boundaries. Note that all the vertices on the offset boundaries are located on the Voronoi edges. In other words, the same Voronoi diagram can be used to compute the offset boundaries for any offset amount. Suppose that the smaller offset corresponds to the offset amount δ_1, and the larger one corresponds to the offset amount $\delta_2 > \delta_1$. Fig. 18b shows the power diagram of the six atoms. Figs. 18c and 18d shows the offset boundaries for δ_1 and δ_2 along with their corresponding power diagrams, respectively. Note that the topological structures of the power diagram in Figs. 18b and 18c are identical, whereas those of Figs. 18b and 18d are different (i.e., the topologies of the tiny edges in the middle of the power diagrams are different). Lemma 7 states this property in terms of dual structure counterpart.

In computational biology, the offset surface is usually called the "solvent accessible surface", and its area is an important parameter that determines solvation energy. In

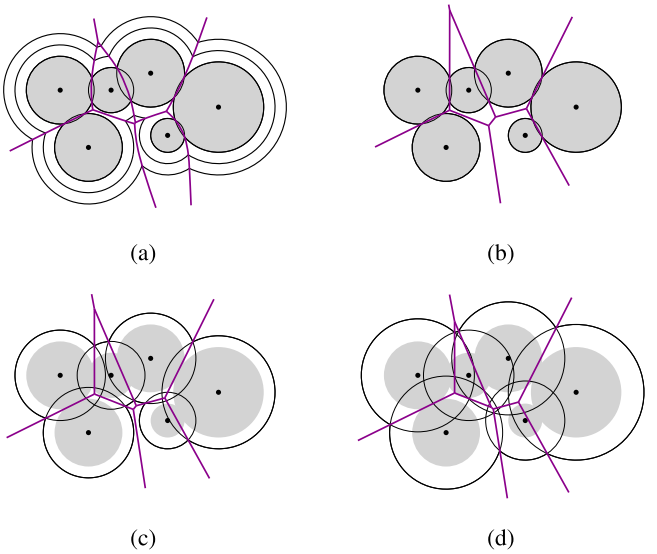

Fig. 18. Different power diagrams are required for different offset amounts for a given molecule. (a) An identical Voronoi diagram is used for different offsets. (b) A power diagram PD_0 necessary for the zero offset amount. (c) A power diagram PD_1 has identical topology to PD_0 (for the offset amount δ_1). (d) A power diagram PD_2 is different from PD_1 (for the offset amount $\delta_2 = 2\delta_1$).

addition, many molecular structure analysis problems are in principle related to the offset surfaces. For example, recognizing molecular voids corresponding to an arbitrary sized probe is an immediate application of this property. Because of its importance for understanding molecular behavior, there have been many studies of void recognition in molecular biology.

7.2 Consequences on Solution Quality

An example that can be easily solved by the beta-complex approach but is hard to solve correctly using the weighted alpha-complex follows.

Problem 2 (Bottleneck Problem). *Let A_1 and A_2 be molecules where $A_1 \cap A_2 = \emptyset$. Compute the minimum Euclidean distance between A_1 and A_2.*

In the beta-complex approach to solve the problem, it is obvious and easy as follows. We first compute the Voronoi diagram of $A_1 \cup A_2$, and collect the *separating Voronoi bisectors* (i.e., Voronoi edges in $\mathbb{R}^2$ or Voronoi faces in $\mathbb{R}^3$) where each bisector has one generating atom from A_1 and the other one from A_2. It is guaranteed that the minimum distance (i.e., the bottleneck) between A_1 and A_2 is given by one of the separating Voronoi bisectors. For each Voronoi bisector, the minimum distance can be computed by the distance between the two defining atoms of the bisector. Hence, this approach is very intuitive, easy, and computationally very efficient.

However, the procedure using the weighted alpha-complex is not so obvious due to the fact that no bisector may be defined at the bottleneck in the power diagram. A possible approach might be to enlarge all the atoms in both A_1 and A_2 by a certain amount, say δ, and see if the enlarged molecules A_1' and A_2' intersect by looking at the power bisectors of the power diagram of $A_1' \cup A_2'$. If A_1' and A_2' do not intersect, we further enlarge both molecules and repeat the intersection check. Suppose that A_1' and A_2' intersect each other. Then, we shrink the two enlarged molecules a little bit so that the intersection amount between the two molecules becomes less than before. By iterating it a sufficient number of times, we may eventually find the situation where the two adjusted molecules touch each other at a single point (in numerical sense). Thus the weighted alpha-complex approach is time consuming and the resulting solution is inevitably an approximation.

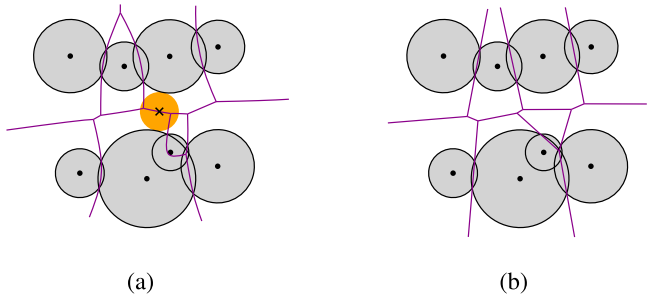

Fig. 19. The difficulty of finding the minimum distance between two molecules in a power diagram. (a) The minimum distance can be easily found in the Voronoi diagram of atoms. (b) No edge is defined in the power diagram between the two atoms of the minimum distance.

Fig. 19 shows a graphical example of the minimum distance computation between two molecules A_1 and A_2 in the plane. Fig. 19a shows the Voronoi diagram of $A_1 \cup A_2$. The orange disk denotes the location where the minimum distance (i.e., bottleneck) occurs. Note that the center of the orange disk is precisely located on the Voronoi edge. Fig. 19b shows the power diagram of the two molecules, and we see that no edge is defined between the two atoms of the minimum distance.

Problem 3 (Cavity Problem). *Given a molecule A, identify cavities such as voids and tunnels. The void is a space where a spherical probe of radius δ in the space cannot move outside without intersection with atoms in A, and the tunnel is a path where the probe can pass through the molecule A.*

The beta-complex approach to solve the problem is very intuitive and easy. We first compute the beta-shape from the Voronoi diagram of of A. Then, we trim off the Voronoi structure lying inside the union of the enlarged atoms A' by δ. In this case, the interior Voronoi structure has one-to-one correspondence with the beta-shape of the parameter $\beta = \delta$. Then, the remaining Voronoi structure is equivalent to molecular exterior and can be used to recognize the tunnels corresponding to the probe. Fig. 1 shows an example of a detected tunnel that the probe of radius $\beta = \delta = 1.4$ can pass through a protein (PDB code: 1jd0). For the details, see [43], [44], [69].

Fig. 20 shows a two-dimensional example to recognize voids and tunnels using bete-shapes for various probe sizes. Fig. 20a shows input atoms and their Voronoi diagram. Fig. 20b shows the beta-shape for a probe of radius β_1 and the corresponding offset of the atoms. The black solid disk denotes the beta-probe. The offset boundary is represented by the chains of red circular arcs. Each vertex and circular arc of the offset boundary corresponds to an edge and a vertex of the beta-shape, respectively. Note that the beta-probe center cannot be located inside the offset, i.e., the shaded region in the figure, but moves outside the offset only. The beta-shape in Fig. 20b consists of three connected components, and therefore the union of enlarged atoms consists of

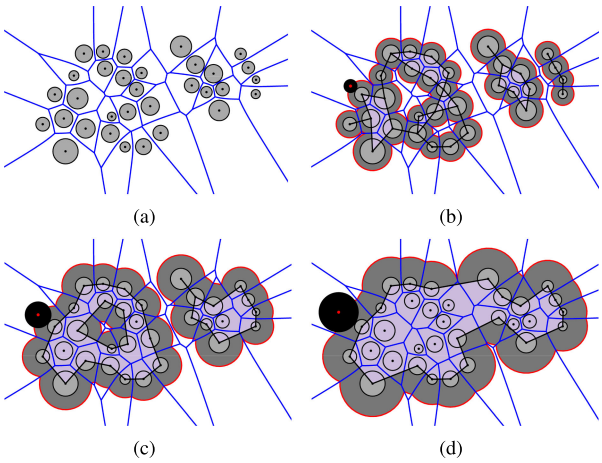

Fig. 20. Efficient recognition of voids, tunnels, and offsets of disks using the unique Voronoi diagram and the beta-shapes. (a) Two-dimensional atoms and the Voronoi diagram. (b) The offset computed from the beta-shape corresponding to the probe radius β_1: Two voids and two tunnels. (c) The offset and the beta-shape for β_2 ($>\beta_1$): The smaller void and narrower tunnel disappeared. (d) the offset and the beta-shape for β_3 ($>\beta_2$): Neither void nor tunnel remains.

the same number of components. There are two tunnels and two voids. The probe can pass through the tunnels between pairs of components. A probe is trapped within and cannot escape from a void. Fig. 20c is the result when bigger probe radius $\beta_2(>\beta_1)$ is used. The new beta-shape has two connected components: The smaller void and the narrower tunnel are disappeared. In Fig. 20d, a much bigger probe radius $\beta_3(>\beta_2)$ is used, and the beta-shape merged into one single component with neither void nor tunnel. Be aware that we use a unique Voronoi diagram and quasi-triangulation for all beta-shapes. However, it is not very obvious how to solve the tunnel recognition problem in the weighted alpha-complex approach unless the power diagram of the inflated molecule is first computed for each value of δ. The computation of the bottleneck seems very hard, too.

Solving this problem has an important implication for significant problems in molecular biology. Tunnel structure is important in cellular molecules: ions pass through ion channels; proteins are synthesized in tunnel structures in ribosome; ribosomal antibiotics usually function in ribosomal tunnels; proteasome disassembles proteins in its tunnel structure, etc. Therefore, recognition of tunnels in biomolecules along with computation of their bottlenecks has many important applications in life science.

The *Cavity Problem* can also be applied to material science to analyze material's property. Fig. 21 shows such an example of recognizing voids in a metallic glass which correspond to several probe radii. Since the atoms are densely packed with a significant level of intersections, only tiny probes can be located in the molecule. Fig. 21a shows a metallic glass consisting of 250 atoms with three different atom types. Figs. 21b, 21c, and 21d show recognized voids with probe radii $\delta = 0.1$Å, $\delta = 0.2$Å, and $\delta = 0.3$Å, respectively. The recognized voids in this figure are represented by the offset surfaces of the three different offset amounts, which is the solution of the *Offset Problem*. We emphasized that, in this example, only one QT and thus one Voronoi diagram is used for the beta-complexes of various δ's.

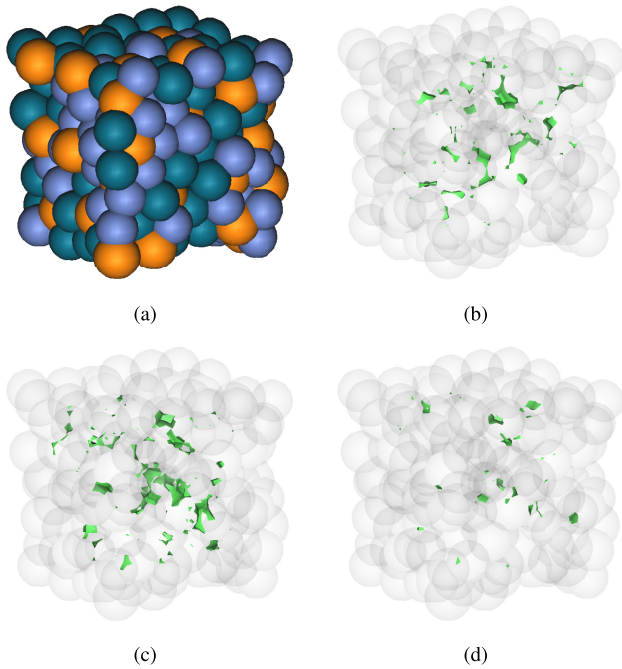

Fig. 21. Metallic glass and the distribution of tiny (green) voids detected using beta-complexes for various beta values. A void is a set of points in the space where each point corresponds to the center of spherical probe that do not intersect atoms. A movie file showing the 3D views of this example is presented as a supplemental material, available online. (a) a metallic glass modelled by 250 spherical atoms (100 Pd's of radius 1.63Å, 100 Ni's of radius 1.63Å, and 50 P's of radius 1.80Å), (b) the voids with parameter $\beta = 0.1$Å, (c) the voids with $\beta = 0.2$Å, and (d) the voids with $\beta = 0.3$Å.

8 Conclusions

Proximity among particles is fundamental for many problems in engineering and science and is critical in structural molecular biology because many problems are in principle proximity ones. While there are similarities between the beta-complex and the (weighted) alpha-complex, the dissimilarity results in a significant consequence in both computational efficiency and solution quality for applications. In this paper, we have shown that the beta-complex is a very intuitive, efficient, and convenient computational construct for the proximity problems among spherical particles such as molecular atoms. Particularly when a problem is related with offset operation in the Euclidean distance, the capability of the beta-complex is far beyond that of the weighted alpha-complex.

Acknowledgments

This work was supported by the National Research Foundation of Korea (NRF) grant funded by the Korea government (MSIP, MSIT) (No. 2017R1A3B1023591, No, 2016K1A4A3914691). The first author (D. Kim) was supported by the Research Grant from Gangneung-Wonju National University.

References

[1] N. Amenta, M. Bern, and M. Kamvysselis, "A new Voronoi-based surface reconstruction algorithm," in *Proc. 25th Annu. Conf. Comput. Graph. Interactive Techn.*, 1998, pp. 415–421.

[2] N. Amenta, S. Choi, and R. K. Kolluri, "The power crust, unions of balls, and the medial axis transform," *Comput. Geom. - Theory Appl.*, vol. 19, pp. 127–153, 2001.

[3] L. Kobbelt and M. Botsch, "A survey of point-based techniques in computer graphics," *Comput. Graph.*, vol. 28, no. 6, pp. 801–814, 2004.

[4] Q. Mérigot, M. Ovsjanikov, and L. Guibas, "Voronoi-based curvature and feature estimation from point clouds," *IEEE Trans. Vis. Comput. Graph.*, vol. 17, no. 6, pp. 743–756, Jun. 2011.

[5] B. Lee and F. M. Richards, "The interpretation of protein structures: Estimation of static accessibility," *J. Mol. Biol.*, vol. 55, pp. 379–400, 1971.

[6] K. P. Peters, J. Fauck, and C. Frömmel, "The automatic search for ligand binding sites in protein of known three dimensional structure using only geometric criteria," *J. Mol. Biol.*, vol. 256, pp. 201–213, 1996.

[7] B. K. Shoichet and I. D. Kuntzt, "Protein docking and complementarity," *J. Mol. Biol.*, vol. 221, pp. 327–346, 1991.

[8] H. Edelsbrunner, M. Facello, and J. Liang, "On the definition and the construction of pockets in macromolecules," *Discr. Appl. Math.*, vol. 88, pp. 83–102, 1998.

[9] J. Liang, H. Edelsbrunner, and C. Woodward, "Anatomy of protein pockets and cavities: Measurement of binding site geometry and implications for ligand design," *Protein Sci.*, vol. 7, no. 9, pp. 1884–1897, 1998.

[10] A. Heifets and M. Eisenstein, "Effect of local shape modifications of molecular surfaces on rigid-body protein-protein docking," *Protein Eng.*, vol. 16, no. 3, pp. 179–185, 2003.

[11] N. Lindow, D. Baum, and H.-C. Hege, "Voronoi-based extraction and visualization of molecular paths," *IEEE Trans. Vis. Comput. Graph.*, vol. 17, no. 12, pp. 2025–2034, Dec. 2011.

[12] J. D. Bernal and J. L. Finney, "Random close-packed hard-sphere model II. Geometry of random packing of hard spheres," *Discussions Faraday Soc.*, vol. 43, pp. 62–69, 1967.

[13] F. M. Richards, "The interpretation of protein structures: Total volume, group volume distributions and packing density," *J. Mol. Biol.*, vol. 82, pp. 1–14, 1974.

[14] D.-S. Kim, C.-I. Won, and J. Bhak, "A proposal for the revision of molecular boundary typology," *J. Biomolecular Struct. Dyn.*, vol. 28, no. 2, pp. 277–287, 2010.

[15] B. J. Gellatly and J. L. Finney, "Calculation of protein volumes: An alternative to the Voronoi procedure," *J. Mol. Biol.*, vol. 161, no. 2, pp. 305–322, 1982.

[16] F. Aurenhammer, "Power diagrams: Properties, algorithms and applications," *SIAM J. Comput.*, vol. 16, pp. 78–96, 1987.

[17] A. Goede, R. Preissner, and C. Frömmel, "Voronoi cell: New method for allocation of space among atoms: Elimination of avoidable errors in calculation of atomic volume," *J. Comput. Chemistry*, vol. 18, no. 9, pp. 1113–1123, 1997.

[18] A. Poupon, "Voronoi and Voronoi-related tessellations in studies of protein structure and interaction," *Current Opinion Struct. Biol.*, vol. 14, pp. 233–241, 2004.

[19] H.-M. Will, "Computation of additively weighted Voronoi cells for applications in molecular biology," Ph.D. dissertation, Department of Computer Science, Swiss Federal Inst. Technol., Zurich, Switzerland, 1999.

[20] D.-S. Kim, D. Kim, and K. Sugihara, "Voronoi diagram of a circle set constructed from Voronoi diagram of a point set," in *Proc. 11th Annu. Int. Symp. Algorithms Comput.*, Dec. 2000, pp. 432–443.

[21] D.-S. Kim, D. Kim, and K. Sugihara, "Voronoi diagram of a circle set from Voronoi diagram of a point set: I. topology," *Comput. Aided Geometric Des.*, vol. 18, pp. 541–562, 2001.

[22] D.-S. Kim, D. Kim, and K. Sugihara, "Voronoi diagram of a circle set from Voronoi diagram of a point set: II. geometry," *Comput. Aided Geometric Des.*, vol. 18, pp. 563–585, 2001.

[23] M. Lee, K. Sugihara, and D.-S. Kim, "Topology-oriented incremental algorithm for the robust construction of the Voronoi diagrams of disks," *ACM Trans. Math. Softw.*, vol. 43, no. 2, pp. 14:1–14:23, 2016.

[24] D.-S. Kim, Y. Cho, and D. Kim, "Edge-tracing algorithm for Euclidean Voronoi diagram of 3D spheres," in *Proc. 16th Can. Conf. Comput. Geom.*, 2004, pp. 176–179.

[25] D.-S. Kim, Y. Cho, and D. Kim, "Euclidean Voronoi diagram of 3D balls and its computation via tracing edges," *Comput.-Aided Des.*, vol. 37, no. 13, pp. 1412–1424, 2005.

[26] D. Kim and D.-S. Kim, "Region-expansion for the Voronoi diagram of 3D spheres," *Comput.-Aided Des.*, vol. 38, no. 5, pp. 417–430, 2006.

[27] Y. Cho, D. Kim, and D.-S. Kim, "Topology representation for the Voronoi diagram of 3D spheres," *Int. J. CAD/CAM*, vol. 5, no. 1, pp. 59–68, 2005, [Online]. Available http://www.ijcc.org.

[28] J. Ryu, D. Kim, Y. Cho, R. Park, and D.-S. Kim, "Computation of molecular surface using Euclidean Voronoi diagram," *Comput.-Aided Des. Appl.*, vol. 2, no. 1/4, pp. 439–438, 2005.

[29] C.-M. Kim, C.-I. Won, Y. Cho, D. Kim, S. Lee, J. Bhak, and D.-S. Kim, "Interaction interfaces in proteins via the Voronoi diagram of atoms," *Comput.-Aided Des.*, vol. 38, no. 11, pp. 1192–1204, 2006.

[30] D.-S. Kim, Y. Cho, D. Kim, S. Kim, J. Bhak, and S.-H. Lee, "Euclidean Voronoi diagrams of 3D spheres and applications to protein structure analysis," *Japan J. Ind. Appl. Math.*, vol. 22, no. 2, pp. 251–265, 2005.

[31] D.-S. Kim, D. Kim, Y. Cho, J. Ryu, C.-H. Cho, J. Y. Park, and H. C. Lee, "Visualization and analysis of protein structures using Euclidean Voronoi diagram of atoms," in *Proc. Int. Conf. Comput. Sci. Appl.*, May 2005, pp. 993–1002.

[32] H. Edelsbrunner, D. G. Kirkpatrick, and R. Seidel, "On the shape of a set of points in the plane," *IEEE Trans. Inf. Theory*, vol. IT-29, no. 4, pp. 551–559, Jul. 1983.

[33] H. Edelsbrunner and E. P. Mücke, "Three-dimensional alpha shapes," *ACM Trans. Graph.*, vol. 13, no. 1, pp. 43–72, 1994.

[34] H. Edelsbrunner, "Weighted alpha shapes," Univ. Illinois at Urbana-Champaign, Urbana, IL, Tech. Rep. UIUCDCS-R-92–1760, 1992.

[35] P. Winter, H. Sterner, and P. Sterner, "Alpha shapes and proteins," in *Proc. 6th Int. Symp. Voronoi Diagrams Sci. Eng.*, Jun. 2009, pp. 217–224.

[36] M. Gameiro, Y. Hiraoka, S. Izumi, M. Kramar, K. Mischaikow, and V. Nanda, "A topological measurement of protein compressibility," *Japan J. Ind. Appl. Math.*, vol. 32, no. 1, pp. 1–17, 2015.

[37] D.-S. Kim, J. Seo, D. Kim, J. Ryu, and C.-H. Cho, "Three-dimensional beta shapes," *Comput.-Aided Des.*, vol. 38, no. 11, pp. 1179–1191, 2006.

[38] D.-S. Kim, Y. Cho, K. Sugihara, J. Ryu, and D. Kim, "Three-dimensional beta-shapes and beta-complexes via quasi-triangulation," *Comput.-Aided Des.*, vol. 42, no. 10, pp. 911–929, 2010.

[39] M. Krone, K. Bidmon, and T. Ertl, "Interactive visualization of molecular surface dynamics," *IEEE Trans. Vis. Comput. Graph.*, vol. 15, no. 6, pp. 1391–1398, Nov./Dec. 2009.

[40] J. Parulek and A. Brambilla, "Fast blending scheme for molecular surface representation," *IEEE Trans. Vis. Comput. Graph.*, vol. 19, no. 12, pp. 2653–2662, Dec. 2013.

[41] S. Grottel, M. Krone, C. Müller, G. Reina, and T. Ertl, "MegaMol–A prototyping framework for particle-based visualization," *IEEE Trans. Vis. Comput. Graph.*, vol. 21, no. 2, pp. 201–214, Feb. 2015.

[42] N. Lindow, D. Baum, and H.-C. Hege, "Ligand excluded surface : A new type of molecular surface," *IEEE Trans. Vis. Comput. Graph.*, vol. 20, no. 12, pp. 2486–2495, Dec. 2014.

[43] D.-S. Kim, Y. Cho, J.-K. Kim, and K. Sugihara, "Tunnels and voids in molecules via Voronoi diagrams and beta-complexes," *Trans. Comput. Sci. XX*, vol. LNCS 8110, pp. 92–111, 2013.

[44] J.-K. Kim, Y. Cho, R. A. Laskowski, S. E. Ryu, K. Sugihara, and D.-S. Kim, "BetaVoid: Molecular voids via beta-complexes and Voronoi diagrams," *Proteins: Struct. Functions Bioinf.*, vol. 82, no. 9, pp. 1829–1849, 2014.

[45] J. Byška, M. L. Muzic, M. E. Gröller, I. Viola, and B. Kozlíková, "AnimoAminoMiner: Exploration of protein tunnels and their properties in molecular dynamics," *IEEE Trans. Vis. Comput. Graph.*, vol. 22, no. 1, pp. 747–756, Jan. 2016.

[46] Y. Cho, J.-K. Kim, J. Ryu, C.-I. Won, C.-M. Kim, D. Kim, and D.-S. Kim, "BetaMol: A molecular modeling, analysis and visualization software based on the beta-complex and the quasi-triangulation," *J. Adv. Mech. Des. Syst. Manuf.*, vol. 6, no. 3, pp. 389–403, 2012.

[47] J.-K. Kim, Y. Cho, D. Kim, and D.-S. Kim, "Voronoi diagrams, quasi-triangulations, and beta-complexes for disks in $\mathbb{R}^2$: The theory and implementation in BetaConcept," *J. Comput. Des. Eng.*, vol. 1, no. 2, pp. 79–87, 2014.

[48] A. Okabe, B. Boots, K. Sugihara, and S. N. Chiu, *Spatial Tessellations: Concepts and Applications of Voronoi Diagrams*, 2nd ed. Chichester, England: John Wiley & Sons, 1999.

[49] F. Aurenhammer, "Voronoi diagrams–A survey of a fundamental geometric data structure," *ACM Comput. Surv.*, vol. 23, no. 3, pp. 345–405, 1991.

[50] Sugihara Homepage, [Online]. Available: http://home.mims.meiji.ac.jp/~sugihara/

[51] CGAL Library Homepage, [Online]. Available: http://www.cgal.org/

[52] K. Mehlhorn and S. Näher, *LEDA: A Platform for Combinatorial and Geometric Computing*. Cambridge, U.K.: Cambridge Univ. Press, 1999.

[53] T. Masada, H. Imai, and K. Imai, "Enumeration of regular triangulations," in *Proc. 12th Annu. Symp. Comput. Geom.*, 1996, pp. 224–233.
[54] H. Edelsbrunner and N. R. Shah, "Incremental topological flipping works for regular triangulation," in *Proc. 18th Annu. Symp. Comput. Geom.*, 1992, pp. 43–52.
[55] M. Gavrilova and J. Rokne, "Updating the topology of the dynamic Voronoi diagram for spheres in Euclidean d-dimensional space," *Comput. Aided Geometric Des.*, vol. 20, no. 4, pp. 231–242, 2003.
[56] V. A. Luchnikov, N. N. Medvedev, L. Oger, and J.-P. Troadec, "Voronoi-Delaunay analysis of voids in systems of nonspherical particles," *Phys. Rev. E*, vol. 59, no. 6, pp. 7205–7212, 1999.
[57] N. N. Medvedev, V. P. Voloshin, V. A. Luchnikov, and M. L. Gavrilova, "An algorithm for three-dimensional Voronoi S-network," *J. Comput. Chemistry*, vol. 27, no. 14, pp. 1676–1692, 2006.
[58] J. Ryu, R. Park, and D.-S. Kim, "Molecular surfaces on proteins via beta shapes," *Comput.-Aided Des.*, vol. 39, no. 12, pp. 1042–1057, 2007.
[59] J. Ryu and D.-S. Kim, "Protein structure optimization by side-chain positioning via beta-complex," *J. Global Optimization*, vol. 57, no. 2, pp. 217–250, 2013.
[60] J.-K. Kim, C.-I. Won, J. Cha, K. Lee, and D.-S. Kim, "Optimal ligand descriptor for pocket recognition based on the beta-shape," *PLoS One*, vol. 10, no. 4, pp. e0 122 787–e0 122 787, 2015.
[61] J.-K. Kim, Y. Cho, M. Lee, R. A. Laskowski, S. E. Ryu, K. Sugihara, and D.-S. Kim, "BetaCavityWeb: A webserver for molecular voids and channels," *Nucleic Acids Res.*, vol. 43, no. W1, pp. W413–W418, 2015.
[62] D.-S. Kim, D. Kim, Y. Cho, and K. Sugihara, "Quasi-triangulation and interworld data structure in three dimensions," *Comput.-Aided Des.*, vol. 38, no. 7, pp. 808–819, 2006.
[63] D.-S. Kim, Y. Cho, J. Ryu, J.-K. Kim, and D. Kim, "Anomalies in quasi-triangulations and beta-complexes of spherical atoms in molecules," *Comput.-Aided Des.*, vol. 45, no. 1, pp. 35–52, 2013.
[64] D.-S. Kim, Y. Cho, and K. Sugihara, "Quasi-worlds and quasi-operators on quasi-triangulations," *Comput.-Aided Des.*, vol. 42, no. 10, pp. 874–888, 2010.
[65] H. Edelsbrunner, "The union of balls and its dual shape," *Discr. Comput. Geom.*, vol. 13, pp. 415–440, 1995.
[66] M. L. Connolly, "Solvent-accessible surfaces of proteins and nucleic acids," *Sci.*, vol. 221, pp. 709–713, 1983.
[67] M. L. Connolly, "Analytical molecular surface calculation," *J. Appl. Crystallography*, vol. 16, pp. 548–558, 1983.
[68] D.-S. Kim, C.-H. Cho, D. Kim, and Y. Cho, "Recognition of docking sites on a protein using β-shape based on Voronoi diagram of atoms," *Comput.-Aided Des.*, vol. 38, no. 5, pp. 431–443, 2006.
[69] D.-S. Kim and K. Sugihara, "Tunnels and voids in molecules via Voronoi diagram," in *Proc. 9th Int. Symp. Voronoi Diagrams Sci. Eng.*, 2012, pp. 138–143.
[70] D.-S. Kim, J. Ryu, H. Shin, and Y. Cho, "Beta-decomposition for the volume and area of the union of three-dimensional balls and their offsets," *J. Comput. Chemistry*, vol. 33, no. 13, pp. 1252–1273, 2012.
[71] D.-S. Kim, J.-K. Kim, Y. Cho, and C.-M. Kim, "Querying simplexes in quasi-triangulation," *Comput.-Aided Des.*, vol. 44, no. 2, pp. 85–98, 2012.
[72] D.-S. Kim, Y. Cho, J.-K. Kim, and J. Ryu, "QTF: Quasi-triangulation file format," *Comput.-Aided Des.*, vol. 44, no. 9, pp. 835–845, 2012.

Donguk Kim received the BS, MS, and PhD degrees from Hanyang University, Seoul, Korea, in 1999, 2001 and 2004, respectively. He is an associate professor with the Department of Industrial and Management Engineering, Gangneung-Wonju National University, Korea. Before he joined the university, he worked as a senior researcher in Voronoi Diagram Research Center, Hanyang University, Seoul, Korea. His current research interests include theory and applications of Voronoi diagrams and their derived data structures in various research areas.

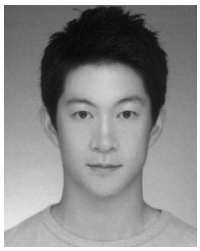

Mokwon Lee received the BS degree from Hanyang University, Seoul, Korea, in 2012. He is currently in the integrated PhD program at the university. His research interests are computational geometry.

Youngsong Cho received the BS, MS, and PhD degrees from Hanyang University, Seoul, Korea, in 1995, 1997, and 2003, respectively. He is a senior researcher in Voronoi Diagram Research Center, Hanyang University, Seoul, Korea. His current research interests include theory and applications of Voronoi diagrams and their derived data structures in various research area.

Deok-Soo Kim received the BS degree from Hanyang University, Korea, and MS degree from the New Jersey Institute of Technology, and the PhD degree from the University of Michigan, in 1982, 1985 and 1990, respectively. He is a professor with the School of Mechanical Engineering, Hanyang University, Korea. Before he joined the university in 1995, he worked at Applicon, USA, and Samsung Advanced Institute of Technology, Korea. His current research interests are theory and applications of Voronoi diagrams and their derived data structures in various research area.